Techno-economic and Life Cycle Assessment of Airport Hydrogen Production Infrastructure for Future Hydrogen-based Aviation

by

Zhen Ye

A thesis

presented to the University of Waterloo

in fulfillment of the

thesis requirement for the degree of

Master of Applied Science

in

Chemical Engineering

Waterloo, Ontario, Canada, 2025

© Zhen Ye 2025

Author's Declaration

This thesis consists of material all of which I authored or co-authored: see Statement of Contributions included in the thesis. This is a true copy of the thesis, including any required final revisions, as accepted by my examiners.

I understand that my thesis may be made electronically available to the public.

Statement of Contributions

Abstract, Chapter 1 and Chapter 2 of the thesis are adopted from a part of a draft manuscript that is under review:

Zhen Ye, Wenrui Ye, John Wen, Xiaoyu. Wu, “Planning renewable hydrogen infrastructure for airports,” Energy, under review, 2025

Wenrui Ye provided the base model and coding support for the preparation of this manuscript. John Wen and XiaoYu Wu initiated the project and are providing guidance with the manuscript.

Abstract

The aviation sector faces growing pressure to reduce emissions, as global air travel continues to expand and jet fuel demand rises. Alternatives such as sustainable aviation fuel (SAF), battery electric, and hydrogen have emerged to reduce dependence on fossil fuels. While SAF offers partial emissions reductions, and electric aviation remains constrained by battery weight and power limitations, hydrogen presents a promising long-term solution. Hydrogen can be used to generate power via combustion or fuel cells, offering the potential for zero carbon emissions. However, implementing hydrogen-based aviation fuel faces challenges, particularly in establishing adequate infrastructure for cost-effective hydrogen production and supply. In addition, it is costly to distribute hydrogen, and early adoption is likely constrained by the availability of a reliable fuel supply chain. This study explores the feasibility of achieving low-carbon hydrogen supply through on-site hydrogen production at airports, integrated with renewable energy sources (RES) and the electrical grid, to increase hydrogen independence and avoid long-distance hydrogen distribution. A mixed-integer linear programming (MILP) model is used to determine the optimal component capacity configuration of the on-site hydrogen facility, considering both economic and energy constraints. Under base-case techno-economic assumptions, an optimal configuration results in an annualized total cost of US$22.7 M and a levelized cost of hydrogen (LCOH) of US$7.45 per kg of liquid hydrogen (LH2). Sensitivity analyses reveal that the system's economic performance and operational patterns are significantly affected by variations in component unit costs and efficiencies. Compared to a system powered solely by RES, integrating grid electricity improves both economic viability and energy efficiency. Simulations using projected parameters for 2050 demonstrate the potential for reducing LCOH reduction while increasing RES utilization. Additionally, life cycle assessment (LCA) of the renewable-based hydrogen infrastructure reveals carbon intensities (CI) between 1.47 and 4.17 kg CO_2-eq/kg LH2, which are 3 to 8 times lower than that of fossil jet fuel, highlighting the environmental benefits of renewable hydrogen. The highest emissions are found to be associated with manufacturing RES and storage components due to the use of fossil fuel in material processing. Results also show trade-offs between economic and environmental performance of renewable hydrogen infrastructure in airports: Wind turbine (WT)-powered configuration offer stronger environmental benefits at a higher cost. This underscores the importance of balancing cost and emission reduction in onsite hydrogen infrastructure design for airports.

Acknowledgements

First and foremost, I would like to express my deepest gratitude to my supervisors, Dr. John Wen and Dr. Xiaoyu Wu, for their invaluable guidance, support, and encouragement throughout the course of this research. From the earliest stages of idea development to the final stages of writing, they provided essential insights that shaped the direction of this thesis. Their expertise, thoughtful feedback, and patience have been instrumental in enhancing the quality and depth of this work.

I would also like to thank the members of my thesis defense committee, Dr. Maxime van der Heijden and Dr. Xianguo Li, for their time, thoughtful questions, and constructive suggestions that have helped improve this thesis.

Special thanks to Dr. Wenrui Ye, who provided expert support on the modeling aspect of this research. His guidance helped me overcome coding challenges and offered valuable advice on renewable energy system modeling.

I am deeply grateful to my wonderful parents for their unwavering support, both financial and emotional, as well as their love and understanding. They have supported me throughout this eleven-year learning journey away from home, from beginning to end. Their belief in me has been a constant source of strength and motivation.

A heartfelt thank you to my girlfriend, Xinge, for her continuous encouragement, emotional support, and patience. Her presence and understanding have made the difficult moments more manageable and the milestones more meaningful. She brings joy to my life every day.

I would like to acknowledge my colleagues from the Laboratory for Emerging Energy Research and the Greener Production Group, who have offered encouragement, companionship, and perspective along the way. Whether through academic discussions or shared moments of relaxation, their support has greatly enriched this experience.

Finally, I would like to thank all my friends outside of academia who have supported me throughout this journey. Your encouragement, humor, and reminders to take breaks have helped me maintain balance and perspective. Whether through late-night conversations, weekend get-togethers, or simply being there when I needed a break, your friendship has played an important role in my well-being and motivation.

Table of Contents

Author's Declaration ii

Statement of Contributions iii

Abstract iv

Acknowledgements v

List of Figures ix

List of Tables xi

List of Abbreviations xiii

List of Symbols xiv

Chapter 1 Background and Literature Review 1

1.1 Hydrogen in Aviation 1

1.1.1 Alternative Aviation Fuel 1

1.1.2 Hydrogen Production 3

1.1.3 Hydrogen Storage for Aviation 6

1.1.4 Hydrogen Refueling 7

1.1.5 Hydrogen Supply for Aviation 8

1.2 Life Cycle Assessment 10

1.3 Motivation and Outline 12

Chapter 2 Techno-economic Analysis of Airport Hydrogen System 14

2.1 Introduction 14

2.2 System Description 14

2.2.1 Energy Supply 14

2.2.2 Hydrogen Subsystem 16

2.2.3 Demand 17

2.2.4 Case Studies 20
2.3 Methodology 20
2.3.1 Objective Function 22
2.3.2 Electricity Supply Constraints 23
2.3.3 Battery System Constraints 24
2.3.4 Gaseous Hydrogen System Constraints 24
2.3.5 Liquid Hydrogen System Constraints 26
2.3.6 Performance Indicators 27
2.4 Results and Discussion 28
2.4.1 2025 Base Case 28
2.4.2 Case Studies 37
2.5 Conclusion 40
Chapter 3 Life Cycle Analysis of Airport Hydrogen System 42
3.1 Introduction 42
3.2 LCA System Description 42
3.3 Life Cycle Inventory Analysis (LCIA) 43
3.3.1 PV Subsystem Inventory 44
3.3.2 WT Subsystem Inventory 45
3.3.3 Electrolyzer Inventory 46
3.3.4 Battery Storage Subsystem Inventory 47
3.3.5 Liquefaction Unit Inventory 48
3.3.6 Storage Subsystem Inventory 48
3.4 Life Cycle Impact Analysis 50
3.5 Results and Discussion 51

3.6 Conclusion 55
Chapter 4 Conclusion and Future Work 57
4.1 Conclusion 57
4.2 Limitation and Future Work 58
References 60
Appendix A . Detailed Life Cycle Inventories and Material Emission Factors 72
Appendix B . Supplementary Sensitivity Analysis Results 83

List of Figures

Figure 2-1. Graphical schematic of hydrogen infrastructure in an airport, including on-site hydrogen production using electrolyzers, gas hydrogen (GH2) storage, liquefaction and LH2 storage, and refueling facility. The yellow arrowhead line corresponds to electricity flow and blue arrowhead line corresponds to hydrogen flow. 16
Figure 2-2. Fuel demand schedule of the Toronto Pearson Airport case-study 18
Figure 2-3. Detailed schematic of energy flow within the airport hydrogen system. The dashed arrowhead line corresponds to flow of AC energy while the solid arrowhead line corresponds to flow of DC energy. The color scheme highlights different subsystems with green corresponding to RES subsystem, yellow corresponding to battery storage, blue corresponding to hydrogen subsystem and red represents grid energy. 21
Figure 2-4, Simulation results for 2025 Base Case; a) Annual energy supply breakdown; b) Hourly energy supply dynamics during moderate renewable availability; c) Hourly energy supply dynamics during high renewable availability; d) Daily energy supply dynamics; e) Weekly energy supply percentage; f) Renewable energy utilization dynamics. 30
Figure 2-5. Impact of change in unit CAPEX of PV, WT and electrolyzer on the results of a). PV sizing, b). WT sizing, c). Electrolyzer sizing, d). GH2 Storage sizing, and e). Electrolyzer utilization. 32
Figure 2-6. Impact of change in unit CAPEX of PV, WT and electrolyzer on the economic results of a). Total annualized component expenditure, b). Annual grid energy cost, and c). LCOH. 34
Figure 2-7. Impact of electrolyzer efficiency on the optimal results, a). System economics performance; b). Renewable and Electrolyzer system sizing; c). GH2 Storage sizing; d). Electrolyzer utilization. 35
Figure 2-8. Impact of unit cost of GH2 storage on the optimal results, a). GH2 Storage sizing; b). Renewable and Electrolyzer system sizing; c). System economics performance; d). Electrolyzer utilization. 36
Figure 2-9. Contribution of system component cost to LCOH for 2025 Base Case, RE-Only, PV-Only, WT-Only and 2050 Case. 38
Figure 3-1. Schematic and system boundary of the well-to-pump life cycle assessment of the airport hydrogen system. 43

Figure 3-2. Component contributions to life cycle CI for RE-Only, PV-Only and WT-Only case studies. 52
Figure 3-3. Material contributions to production CI for the functional unit of Electrolyzer, GH2 storage, PV and WT. 53

List of Tables

Table 2-1. 2025 Base Case techno-economic parameters of the system components. The numbers in parentheses indicate the techno-economic predictions for the 2050 Case. 19
Table 2-2. Summary of case study configurations used in this work. 20
Table 2-3, Summary and comparison of simulation results for the 2025 Base Case, RE Only, PV Only, WT Only cases and 2050 Case. The top section of the table summarizes the results for system component capacities; the middle section shows the overall system cost and the breakdown of system component costs; and the bottom section presents the technical indicators for case study performance assessment. 29
Table 3-1. Summary of life cycle inventory of 1 kW PV functional unit (values adopted from [100], [101]). 44
Table 3-2. Summary of life cycle inventory of 1.65 MW WT functional unit (values adopted from [103]). 45
Table 3-3. Summary of life cycle inventory of 1 MW PEM electrolyzer functional unit (values adopted from [104]) 46
Table 3-4. Summary of life cycle inventory of 2.4 MWh BESS functional unit (values adopted from GREET [101]). 47
Table 3-5. Life cycle inventory of hydrogen liquefaction system of various capacities. 48
Table 3-6. Life cycle inventories of hydrogen storage system components, Top: Compressor (adopted from [75]); Mid: GH2 lined rock cavern storage; Bottom: LH2 storage tank. 50
Table 3-7. Summary of life cycle CI comparison between this study and: Top, literature values per kg H_2; Bottom, jet fuel on a per kWh basis. 55

Table A 1 Detailed life cycle inventory of material requirements of different stages of PV panel production and BOP. 73
Table A 2. Detailed life cycle inventory of material requirements of different parts of WT production and BOP. 75
Table A 3. Detailed life cycle inventory of material requirements of different parts and BOP of PEM electrolyzer stack. 77
Table A 4. Detailed life cycle inventory of material requirements of battery cell and BOP of battery energy system. 79

Table A 5. Emission factor database of materials involved in the LCIs of airport hydrogen system components..... 80

Table B 1. Results of liquefaction unit sizing, LH2 storage capacity and EIS from sensitivity analyses. 84

List of Abbreviations

AEL	Alkaline electrolysis
AEM	Anion membrane electrolysis
ATR	Autothermal reforming
BESS	Battery energy storage subsystem
BOM	Bill of material
BOP	Balance of plant
CCS	Carbon capture and storage
CG	Coal gasification
CI	Carbon intensity
DGME	Dipropylene glycol monomethyl ether
EIS	Energy independent score
GH2	Gaseous hydrogen
HDPE	High-Density Polyethylene
HESS	Hydrogen energy subsystem
LCA	Life cycle analysis
LCI	Life cycle inventory
LCIA	Life cycle inventory analysis
LCOH	Levelized cost of hydrogen
LH2	Liquid hydrogen
PEM	Proton exchange membrane
PET	Polyethylene terephthalate
POX	Partial oxidation
PP	Polypropylene
PTFE	Polytetrafluoroethylene
PV	Photovoltaic panel
RES	Renewable energy source
SAF	Sustainable aviation fuel
SMR	Steam methane reforming
SOEC	Solid oxide electrolysis cell
SR	Steam reforming
WGS	Water-gas shift reaction
WT	Wind turbine

List of Symbols

Latin letters		
$Batt$	Battery	-
$B_{Char,i}$	Boolean value for battery charging at time i	-
$B_{Dis,i}$	Boolean value for battery discharging at time i	-
CAP_j	Capacity of system component j	kW, kWh
$Char$	Charge	-
$Comp$	Compressor	-
$Conv$	Converter	-
$C^U_{C,j}$	Unit capital expenditure of system component j	US$/kW, US$/kWh
$C^U_{C,A,j}$	Annualized unit capital expenditure of system component j	US$/kW, US$/kWh
$C^U_{C,A,j}$	Grid energy imported to the system at time	US$/kW, US$/kWh
$C^U_{FO,j}$	Unit fixed operating expenditure of system component j	US$/kW, US$/kWh
C_{Grid}	Overall cost of gid energy import to the system	US$
$C^U_{Grid,i}$	Unit cost of grid energy import to the system at time i	US$/kWh
$C_{T,A,j}$	Annualized total expenditure of system component j	US$
$C^U_{T,A,j}$	Annualized total unit expenditure of system component j	US$/kW, US$/kWh
Dis	Discharge	-
dr	Discount rate	-
E	Energy flow in the system	kWh
EIS	Energy independent score	-
El	Electrolyzer	-
$E_{Batt,i}$	Energy level in battery at time i	kWh
$E_{Batt_El,i}$	Batter energy flow to electrolyzer at time i	kWh
$E_{Char,i}$	Energy charged to battery at time i	kWh
$E_{Comp,i}$	Compressor energy consumption at time i	kWh
$E_{Dis,i}$	Energy discharged from battery at time i	kWh
$E_{El,i}$	Electrolyzer energy consumption at time i	kWh
$E_{ElDemand,i}$	Energy demand from electrolyzer at time i	kWh
$E_{Fuel,i}$	Fuel demand from flights in energy at time i	kWh
$E_{GH2Stg,i}$	Energy level inside GH2 storage at time i	kWh
$E_{Grid,i}$	Grid energy import to the system	kWh
$E_{Grid_Batt,i}$	Grid energy flow to battery at time i	kWh
$E_{Grid_El,i}$	Grid energy flow to electrolyzer at time i	kWh
$E_{Grid_Liq,i}$	Grid energy flow to liquefaction unit at time i	kWh
$E_{Grid_Comp,i}$	Grid energy flow to compressor at time i	kWh
$E_{LiqDemand,i}$	Energy demand from liquefaction unit at time i	kWh
$E_{LH2\ ,i}$	LH2 generation demand at time i	kWh
$E_{LH2,Stg,i}$	Energy level inside LH2 storage at time i	kWh
$E_{PV_curt,i}$	Curtailed PV energy at time i	kWh
$E_{PV_RE,i}$	PV energy flow into the system at time i	kWh
$E_{RE_Batt,i}$	Renewable energy flow to battery at time i	kWh

$E_{RE_Comp,i}$	Renewable energy flow to compressor at time i	kWh
$E_{RE_El,i}$	Renewable energy flow to electrolyzer at time i	kWh
$E_{RE_Liq,i}$	Renewable energy flow to liquefaction unit at time i	kWh
$E_{WT_RE,i}$	WT energy flow into the system at time i	kWh
$E_{WT_curt,i}$	Curtailed WT energy at time i	kWh
$Fuel$	Hydrogen aviation fuel	-
f_{CR}	Capital recovery factor	-
$f_{FO,j}$	Fixed operating expenditure factor	-
$GH2Stg$	GH2 storage	-
HES	Hydrogen energy subsystem	-
i	Set of simulation time in hour	hr
Inv	Inverter	-
j	Set of system component	-
$LCOH$	Levelized cost of hydrogen	US$/kg LH2
Liq	Liquefaction unit	-
$LH2Stg$	LH_2 storage	-
LT	System component lifetime	years
M	An arbitrary large number to enforce constraints in MILP	-
PV	Photovoltaic panel	-
R_C	Renewable curtailment ratio	-
SEC_j	Specific energy consumption of component j	kWh/kg H_2
U_E	Utilization of electrolyzer	-
U_L	Utilization of liquefaction unit	-
WT	Wind turbine	-

Greek letters

η_{Batt}	Roundtrip battery efficiency	-
η_{Comp}	Compressor loss coefficient	-
η_{Conv}	Converter efficiency	-
η_{El}	Electrolyzer efficiency	-
η_{Inv}	Inverter efficiency	-
η_{LH2}	LH2 storage loss	-

Chapter 1 Background and Literature Review

1.1 Hydrogen in Aviation

1.1.1 Alternative Aviation Fuel

The aviation industry has experienced consistent growth, with the number of global air passengers reaching 4.6 billion in 2019 [1]. This rapid expansion has inflicted significantly energy consumption, e.g., the US commercial airlines using an estimated 18.2 billion gallons of jet fuel in 2019 alone [2]. Kerosene-based jet fuel is derived primarily from fossil fuels like crude oil. In 2019, the US petroleum product supply averaged around 17.3 million barrels per day, of which daily jet fuel supply accounted for around 10%, or 1.74 million barrels per day [3]. This rising demand for jet fuel accelerates the depletion of finite fossil fuel resources and raises concerns about emissions. In 2019, the global aviation sector produced approximately 1.02 Gt of CO_2 emissions[4], which accounted for about 3% of total global CO_2 emissions (i.e., 33.3 Gt [5]). Besides CO_2, NO_x from jet engines is another significant aviation-related emission. The high-temperature combustion of kerosene produces NO_x, which is released into the stratosphere where it accelerates the depletion of both tropospheric and stratospheric ozone, while also contributing to the formation of acid rain and smog [6]. These environmental concerns, along with the growing reliance on non-renewable energy sources, highlight the need for alternative fuels to replace fossil jet fuel, with notable options including SAF, battery electric, solar electric, and hydrogen [7].

Among these options, SAF is one of the most established alternatives, with several technologies available and some already commercialized. SAF is produced by synthesizing kerosene from carbon-based biomass such as carbohydrate-based feedstocks (e.g., algae biomass, sugarcane), lignocellulosic feedstocks (e.g., forestry waste, straw), and oil-based feedstocks (e.g., used cooking oil, animal fat, food waste) [7], [8]. The renewable nature of these feedstocks allows SAF to replace depleting fossil resources like oil and gas. Hydroprocessed esters and fatty acids (HEFA) are a well-established and commercialized process that converts oil-based feedstocks into hydrocarbon fuels through deoxygenation and hydrotreating [9], [10], [11]. Other methods that are close to commercial readiness include the Fischer–Tropsch (FT) process, which converts synthesis gas from feedstock gasification into hydrocarbon fuels, and the alcohol-to-jet (ATJ) pathway, which converts alcohol from fermented carbohydrate-based feedstocks into jet-fuel-grade kerosene [10]. There are also technologies at lower technology readiness level and under research including direct sugars to hydrocarbons (DSHC) and aqueous phase reforming (APR) [10]. Although SAF still emits CO_2 during flight, bio-feedstocks, such as algae and sugarcane, absorb CO_2 during growth, offering the

potential towards net-zero emissions over the fuel's life cycle [9]. Life cycle assessments of International Civil Aviation Organization (ICAO)-eligible SAFs have shown 26% to 94% reductions in life cycle CO_2 emissions, and a report by the Royal Netherlands Aerospace Centre (NLR) estimates that SAF use in Europe could cut aviation CO_2 emissions by up to 46% by 2050 [10].

Battery electric technology has been widely researched for aviation, as using green electricity reduces fossil fuel demand. Battery-electric aircraft use battery packs and electric motors, with the motor drawing electricity from the battery to drive the propeller and propel the aircraft [12]. Research has also explored hybrid electric aircraft to improve fuel efficiency and reduce emissions [12]. However, electric aviation remains at the proof-of-concept stage, e.g., projects like NASA's Maxwell and Eviation's Alice [13], [14]. Major challenges include the heavy weight of batteries, which have much lower energy density than kerosene (0.35 kWh/kg vs. 12 kWh/kg) [7]. Even with emerging Li-S or Li-Air batteries reaching 1 to 3.5 kWh/kg [7], [15], electric aircraft would still be heavy, reducing the paid-load or range. Another limitation is the low power of current electric aviation motors. For example, the state-of-the-art motor developed by Airbus for the E-FAN X project produces 2 MW [16], whereas a turbofan engine for a wide-body aircraft like the A330 generates around 40 MW [12], which is 20 times more power. Although fully electric aircraft powered by green electricity could achieve true zero emissions during flight, the NLR report estimates that electric and hybrid aircraft, combined with novel jet fuels, would only reduce EU aviation emissions by 17% by 2050 due to limited deployment scenarios [10].

Hydrogen alternatives are still in the early stages of research for aviation, although the concept of hydrogen-powered airplanes has existed since the latter half of the last century. The US experimented with the Air Force's B-57 hydrogen demonstrator in 1957, and the Soviets tested hydrogen combustion propulsion with a Tupolev TU-155 test plane in 1988 [17]. Research into hydrogen aviation has re-emerged in recent years as advancements in electrolyzers and renewable electricity technologies increase the feasibility of green hydrogen [18]. Notably, Airbus announced its ZeroE Program in 2020, aiming to introduce a hydrogen-powered airliner with a range of approximately 1,800 km and a capacity of 100 passengers by 2035 [19]. In 2021, De Havilland Canada signed a memorandum of understanding (MOU) with hydrogen aircraft engine developer ZeroAvia to develop a hydrogen powertrain for the DH-8 series airliner [20]. In general, there are two ways to use hydrogen as an aviation fuel: combustion and fuel cells. Hydrogen can replace kerosene in gas turbine engines [17], [21]. On the other hand, hydrogen fuel cells can generate electricity to drive the motor to power the propeller in aircrafts [17], [21]. Both approaches offer carbon-free operations, producing water as the primary byproduct [17], [21]. While fuel cells provide zero emissions,

combustion engines fueled by hydrogen still produce NO_x due to high combustion temperatures [17], [21]. According to the NLR report, increasing adoption of hydrogen fuel is expected to reduce carbon emissions in the aviation sector by over 21% by 2050 [10].

1.1.2 Hydrogen Production

Steam reforming (SR) is a widely used method for hydrogen production that involves a catalytic reaction with nickel-based catalysts at high temperatures ranging from 800 to 900 °C, using light hydrocarbon fuels such as methane, ethane, propane, and naphtha [22], [23]. The most commonly used fuel in SR is methane, which is known as steam methane reforming (SMR), while research has also suggested the use of syngas derived from biomass gasification as a feedstock for the SR process, making it a more sustainable option based on renewable sources [22], [24]. The process consists of two main stages: syngas generation through reforming and carbon monoxide conversion via the water-gas shift (WGS) reaction [22], [23]. To achieve higher hydrogen purity, an additional purification stage is often included, typically involving CO_2 removal through adsorption techniques [22]. While SMR is economically favorable and well-suited for large-scale hydrogen production, it generates significant CO_2 emissions due to its reliance on fossil fuels. Consequently, integrating carbon capture and storage (CCS) technologies with SMR has become a major research focus, as it can reduce greenhouse gas emissions, albeit the process introduces additional energy consumption [22], [25].

Partial oxidation (POX) is an exothermic process in which hydrocarbons such as methane, naphtha, or heavier fuels like residual oil and coal react with pure oxygen to produce hydrogen and carbon oxides [22]. The POX of coal is also commonly referred to as coal gasification (CG), which is widely adopted in countries with abundant coal resources, such as China [23]. Since the reaction releases heat, it does not require external heating sources, making it relatively energy efficient. POX can operate in two modes: the catalytic process, which typically runs at around 950 °C and uses lighter feedstocks like methane, and the non-catalytic process, which operates at 1150–1315 °C and is suitable for heavier hydrocarbons [23]. While POX is reported to have higher tolerance to sulfur impurities and is more appropriate for feedstocks with lower hydrogen-to-carbon ratios, it requires pure oxygen instead of air, as nitrogen in air increases the cost of downstream gas separation [22]. Overall, the POX method is capital-intensive due to the costs of oxygen production and desulfurization, and it is less commonly used than SR because of its lower hydrogen yield and high initial investment [22], [23].

The use of SR and POX has enabled cost-effective and large-scale hydrogen production from fossil fuels but comes with significant CO_2 emissions. The growing demand for clean and sustainable energy highlights the need for cleaner hydrogen production methods. Water-splitting technologies have the potential to offer a more environmentally friendly alternative compared to SR and POX. Electrolysis is a well-known and effective water splitting method that decomposes water into hydrogen and oxygen using electrical energy [23]. There are many electrolyzer technologies available, with three of the most researched being alkaline electrolysis, proton exchange membrane (PEM) electrolysis, and solid oxide electrolyzer cell (SOEC) [18], [22], [23]. Among these, SOEC is the most recent, emerging in the 1980s, which is a high-temperature technology that uses both electricity and heat to efficiently produce hydrogen by splitting steam at 500–1000°C, reducing electrical energy needs [18]. It employs an yttria-stabilized zirconia electrolyte with oxygen ions as charge carriers, differing from other electrolysis methods [18], [23]. While promising for large-scale hydrogen production, SOEC has a limited commercial presence, with challenges in material durability due to harsh operating conditions [18].

Alkaline and PEM electrolyzers are the most commercially mature technologies for hydrogen production. Alkaline electrolyzers (AEL), developed over a century ago, are widely used due to their low cost, non-noble metal catalysts, and long operational life [18]. AEL operates with electrodes submerged in a concentrated alkaline solution, using a porous diaphragm to separate gases and transport hydroxide ions [18]. However, AEL faces limitations such as low load flexibility, limited current density, and low-pressure operation [18], [23]. Despite these drawbacks, it remains a dominant and cost-effective option for large-scale hydrogen production [23].

PEM electrolyzers offer several advantages over traditional alkaline systems, including higher current densities, faster dynamic response, wider partial load range, and higher hydrogen purity, making them well-suited for integration with RES (RES) [18]. Operating in an acidic environment with a solid polymer membrane, PEM systems use protons as charge carriers and allow for compact, efficient designs [18]. However, they rely on expensive noble metal catalysts such as platinum and iridium and face challenges with shorter lifespans due to membrane degradation [18]. To improve cost-effectiveness and durability, ongoing research focuses on alternative materials like nanofiber membranes and non-noble metal catalysts, aiming to enhance PEM electrolysis performance and accelerate its commercial viability for large-scale hydrogen production [18], [23].

Other emerging electrolysis technologies are also under development, aiming to provide more cost-effective solutions for clean hydrogen production. Among them is anion exchange membrane (AEM) electrolysis, which combines features of both AEL and PEM, using a solid polymer electrolyte to separate the electrodes and operate under alkaline conditions [26]. Compared to PEM, AEM has the potential to offer lower capital costs, as it does not require precious metal catalysts [26]. It has also been reported that AEM can operate using low-concentration alkaline solutions, which are less corrosive than the concentrated KOH used in AEL, provide additional safety in operation [26]. Despite these advantages, the technology readiness level of AEM is less mature than that of PEM or AEL, with challenges such as low ionic conductivity and poor catalyst stability [26], [27].

Another known water splitting method is thermolysis, which involves extremely high temperatures of over 2500 °C to split water into hydrogen and oxygen, making it impractical with sustainable energy sources due to cost and material challenges [22]. To address this, thermochemical water-splitting cycles have been developed as a more feasible alternative, using a series of chemical reactions to produce hydrogen at lower temperatures (typically above 550 °C) [23]. These cycles can be powered by solar or nuclear heat, with systems like the S-I (sulfur–iodine) and Cu–Cl (copper–chlorine) cycles among the most promising due to their relatively lower temperature requirements and lack of greenhouse gas emissions [23]. Currently the method is not used at a large scale, with challenges in material degradation from the high process temperature as well as other design challenges in solar energy integration and process control [23].

Apart from thermolysis, other emerging technologies are also hot research topics aimed at providing cleaner and more efficient methods for hydrogen production. Pyrolysis is an emerging technology for producing hydrogen from hydrocarbon fuels, with methane being the most favorable feedstock [22], [23]. Unlike SR, pyrolysis involves only hydrocarbons in the process, where the fuel is thermally decomposed into solid carbon and hydrogen at high temperatures [22]. Compared to SMR, methane pyrolysis is reported to require less energy per unit of hydrogen produced [22]. Since the byproduct is solid carbon rather than CO_2, the process does not require a CCS stage, making it both less energy-intensive and potentially cleaner. However, pyrolysis has not yet been adopted at large scale due to technical challenges, particularly in separating and purifying the hydrogen product [23].

Autothermal reforming (ATR) is another emerging method that integrates the benefits of POX and steam reforming in a single reactor by using the heat from partial oxidation to drive the endothermic steam reforming reaction, maintaining thermal equilibrium within the system [22]. It requires the use of both

steam and air. ATR is still in the developmental stage and not yet commercially deployed on a large scale as research continues in the exploration of reactor designs and catalyst optimization [22].

The use of bioconversion is also among the emerging technologies, which involves using microorganisms to synthesize hydrogen through biochemical processes [23]. Typical methods of bioconversion include biophotolysis and fermentation [23]. The bioconversion processes are promising due to their environmentally friendly nature, however, these methods have proven difficult to scale up due to the limited yield of hydrogen [23].

1.1.3 Hydrogen Storage for Aviation

Although still at the proof-of-concept stage, hydrogen propulsion has great potential in aviation due to several advantages over kerosene and other alternative fuels. One advantage is hydrogen's high energy density by weight, approximately 33 kWh/kg [21], [28]. This is not only significantly higher than the prospective battery energy density (3.3 kWh/kg for a theoretical Li-Air battery [15]) but also higher than kerosene (12 kWh/kg) [21], [28]. This allows hydrogen-powered airplanes to carry less fuel by weight to cover the same trips as their kerosene counterparts. Yet hydrogen-powered aviation still faces significant challenges with fuel storage for both on board and at the airport. While hydrogen's gravimetric energy density (33 kWh/kg) is higher than that of kerosene (12 kWh/kg), its volumetric energy density is quite low. The volumetric energy density of hydrogen is 2.4 kWh/L at a liquid state [21], [28], much lower than kerosene's 10.4 kWh/L [21], [28]. In other words, LH2 requires a storage volume which is about five times that of kerosene to store the same amount of energy on board. The volumetric energy density of compressed hydrogen gas is even lower, at around 1.4 kWh/L at 700 bar [28]. This poses challenges for designing onboard storage systems for hydrogen fuel. To minimize onboard fuel storage size, research suggests that hydrogen should be stored in its liquid state on board for aviation [17].

The low volumetric density creates design challenges, as larger storage systems must be incorporated into fuselage. Current aircraft designs store fuel in the wings, but LH2's volume requirements require alternative storage locations. Some proposed designs suggest replacing some valuable cargo space for hydrogen storage, while more innovative concepts consider blended-wing fuselages for the new fuel type [17]. LH2 storage also brings material and safety challenges. Known as a cryogenic fuel due to its extremely low boiling point (20 K) [29], LH2 requires specially designed tanks made from materials capable of withstanding these temperatures. These storage systems tend to be very heavy with current materials and designs, potentially offsetting hydrogen's gravimetric energy density advantage [21]. Although LH2 has

safety advantages over kerosene, such as a low flammability limit and high auto-ignition temperature, its cryogenic properties require careful safety measures [7], [29]. Under cryogenic conditions, LH2 is extremely volatile and has a high boil-off rate, which can cause overpressure if not properly managed [7], [29]. Consequently, boil-off handling procedures must be part of the storage system, increasing its weight and complexity.

At the terminal, hydrogen can be stored in its gaseous state in either aboveground or underground storage. Aboveground gaseous hydrogen (GH2) storage uses compressed hydrogen tanks with pressures ranging from 200 to 700 bar to optimize storage density [30], [31]. Underground GH2 storage utilizes salt caverns or rock caverns, with storage pressures ranging from 100 to 200 bar [32], [33]. The storage of LH2 utilizes cryogenic tanks with optimized geometric design and insulation to maintain storage conditions without requiring additional energy input for refrigeration. A spherical tank shape is considered optimal for cryogenic storage due to its minimal surface area for heat transfer [34]. Cryogenic tanks also feature double- to triple-layered spaced-wall construction with additional heat-shielding materials to minimize various forms of heat transfer [34], though boil-off still occurs overtime[35].

1.1.4 Hydrogen Refueling

Hydrogen refueling technology has also been extensively researched, particularly in the context of road vehicles[36], [37]. There are two types of refueling strategies: on-site and off-site refueling stations. On-site refueling stations include hydrogen generation facilities alongside refueling dispensers. Common technologies for on-site hydrogen generation include water electrolysis and steam methane reforming (SMR) [37]. Water electrolysis can utilize renewable electricity generated nearby or on-site, enabling greener hydrogen production [37]. In contrast, off-site refueling stations operate similarly to traditional gasoline stations, with hydrogen transported from production sites [36], [37].

Early investigations into hydrogen refueling systems for aviation date back to the late 1970s, when several research works conducted by NASA and Lockheed Martin [38], [39], [40] on the technical assessment for hydrogen aircraft operation and refueling facilities design in airports. These works provided technical details on airport hydrogen facilities and hydrogen aircraft designs regarding the available technologies at the time [38], [39], [40]. Later in the 1980s, Jones et al. modeled the technical details of LH2 pipeline for airport distribution [9]. Recently, a renewed interest in hydrogen-based aviation has led to more detailed analyses on hydrogen infrastructure in airports, not only focusing on the technical assessments of system components but also analyzing the environmental and economic aspects of the topic. Sefain from Cranefield

University provided a comprehensive study on hydrogen aviation, including aircraft certification, ground operations, LH2 fuel production and operation economic analysis [42]. Janic outlined the production and distribution requirements for hydrogen based commercial air transportation along with a model to evaluate the greenhouse gas (GHG) emission of hydrogen air transportation [43]. The feasibility of introducing hydrogen airplane into airport traffic was provided by Haglind et al [44], who estimated the fuel demand of hydrogen aviation in Sweden and evaluated the pathways of producing hydrogen, including water electrolysis, steam methane reforming (SMR) and biomass gasification. Fusaro et al. assessed the economics, and environment impacts for hydrogen-based hypersonic aviation [45], and evaluated the cost of hydrogen production and liquefaction for hypersonic aircraft. Their study suggested that the environmental impact of hydrogen production using electricity from fossil fuel is worse than that from SMR [45]. A study by Mangold et al. designed and analyzed the refueling procedure of hydrogen aircraft during turnaround [46], and reported that LH2 fuel has the advantage in shorter fueling time at large quantities compared to kerosene fuel. A detailed techno-economic assessment of hydrogen infrastructure in airport is provided by Holzen et al [47]. They developed a mixed-integer linear (MILP) model which provides economic optimization and topology for LH2 facilities in the airport [47]. Their work assessed the demand scenarios for various airport capacities and suggested that airports with annual demand over 100 kt LH2 has the potential to take the role of special H_2 hub in its region [47]. Currently, the existing literature on hydrogen airports has already addressed various aspects of hydrogen-powered aviation. Numerous studies have investigated the technical feasibility and environmental impact of implementing hydrogen technologies in aviation. Recent research has also assessed the techno-economic feasibility of hydrogen airport designs, primarily focusing on high-demand scenarios with significant market penetration of hydrogen aircraft in the aviation industry [35], [47].

1.1.5 Hydrogen Supply for Aviation

Hydrogen can be distributed in various ways. A frequently suggested method is road transport, where hydrogen is delivered via compressed tube trailers in gaseous form or liquid tankers in liquid form [36]. The payload size of both gaseous and LH2 transport is limited by its low volumetric energy density [36]. For gaseous hydrogen (GH2), transport pressures typically do not exceed 50 MPa, with an expected delivery amount of approximately 1,000 kg per trip. LH2, due to its higher energy density, allows for a delivery quantity up to four times greater than GH2 [36], [37]. However, satisfying the large fuel demand of an airport with road transport alone is challenging. Pipeline transport, offering larger delivery quantities and lower delivery pressures compared to road transport, is another commonly mentioned method [36], [37].

Pipeline transport also has lower operating costs once infrastructure is established [36], [37]. However, the high initial cost of building hydrogen pipelines hinders their expansion. To address this issue, researchers have suggested using existing natural gas pipelines for hydrogen distribution by mixing hydrogen and natural gas during operation [48]. Novel delivery methods have also emerged for hydrogen transport, including liquid organic carriers, metal hydrides, and hydrogen-to-ammonia systems [36], [37].

The hydrogen supply chain has therefore been studied to search for the optimized geographical location of production site and distribution method of hydrogen for industrial or refueling purposes [49], [50], [51], [52]. The levelized cost of hydrogen delivery is an important concept for hydrogen applications, as the distribution cost can range from US$2.73/kg to US$8.02/kg across different scenarios [53], which is similar to the production cost of electrolytic hydrogen [54]. Additionally, researchers have examined the optimization of hydrogen supply to airports produced from RES [35], [55]. For hydrogen use in the airport, a recent work by Holzen et al. modeled hydrogen supply chain pathways to airport using a non-linear optimization model [35]. Their work analyzed different pathways including on-site generation and off-site production of hydrogen using RES. The work reported that the cost of transporting off-site LH2 to airports can be more than US$2.5/kg and the cost of GH2 transport with pipeline can be more than US$4/kg at a low annual LH2 demand of less than 100 kt. With a very high demand of over 1000 kt annually, the transporting cost of both LH2 and GH2 can be reduced to less than US$1/kg. Robles et. al designed and analyzed the hydrogen supply chain for an airport ecosystem [55]. Their work uses MILP models to find the optimal design minimizing hydrogen cost and CO_2 emissions for the hydrogen-based airport ecosystem in the Hautes-Pyrénées region. Results reported a delivered hydrogen cost of over US$20/kg in 2020 across different scenarios, which will reduce to less than US$4/kg by 2050. Cybulsky adopted a different approach, conducting a techno-economic study on a large-scale aviation hydrogen supply chain set in Europe in 2040 using a decision optimization method, and reported an average LCOH of up to 2 €/kg across different scenarios [56]. Another study by Alexandrou and Khatiwada, which focused on aviation hydrogen supply chains in the French region, reported LCOHs in 2025 of 13.10 €/kg H_2 for pipeline delivery and 10.92 €/kg H_2 for trailer truck delivery, with delivery costs accounting for 3.35 €/kg H_2 and 0.47 €/kg H_2, respectively [57].

The above studies all assumed a high hydrogen aircraft adoption rate with regular hydrogen refueling needs. Yet in the early-stage implementation of hydrogen-powered commercial aviation or small airports with limited-service regions and specific aircraft models, different combinations of hydrogen production and storage capacity may be required and the operation in a small-scale hydrogen infrastructure with a limited

demand can be different from that on a large-scale. In addition, modeling hydrogen infrastructure in airports requires detailed specifications of the supporting systems for hydrogen production, storage and refueling. Yet during the initial design stage, a lack of infrastructure information is anticipated to hinder the hydrogen supply chain to airports, and several studies have shown that the cost of establishing supply infrastructure will be significantly high [35], [53]. More recently, Schenke et al. used linear optimization to model LH2 infrastructure for the early phase of hydrogen-powered aviation, focusing on suitable hydrogen supply routes for airports with low aircraft traffic [58]. They found on-site LH2 production to be cost-effective for small demands and suggest regional airport as promising first movers due to lower space constraints and proximity to renewable resources or other hydrogen users [58]. Another recent study by Rezaei et al. examined a similar system set in the LAX (Los Angeles International Airport) area, using only RES to supply the on-site hydrogen production systems, and reported an LCOH of up to US$7.10/kg H_2 in 2030, with the value projected to decrease to US$3.78/kg H_2 by 2050 [59]. Consequently, it is likely that airports will need to rely on self-sufficient hydrogen production on-site to address the limited supply chain at an early-adoption stage. This is like a microgrid, where hydrogen has been studied as an energy storage medium [60], [61], [62] or as a locally produced fuel for fuel cell electric vehicles (FCEV) refueling [63], [64], [65]. The former works mainly focused on the optimization of system component capacities or the optimized energy management strategies between the RES and different storage mediums. The latter works aimed to find the optimal size of hydrogen production system, especially the electrolyzer, to satisfy the demand of road vehicles refueling while minimizing the levelized cost of hydrogen at the dispenser.

1.2 Life Cycle Assessment

Life cycle assessment (LCA) is a widely used methodology for assessing and comparing the environmental impacts of products by evaluating their entire life cycle, encompassing all stages from raw material extraction, manufacturing, service, and operation to end-of-life disposal. The LCA approach is guided by the principles outlined in ISO 14044 standards, which define the four key phases: goal and scope definition, inventory analysis, impact assessment, and interpretation [66].

A growing number of LCA studies aimed at evaluating the environmental impacts of adopting hydrogen-based technologies. Numerous studies have been conducted to compare the life cycle impacts of various hydrogen production methods. Cetinkaya et al. conducted an LCA of hydrogen vehicle fuel produced via several pathways, including SMR, coal gasification, thermal water splitting, and electrolysis [67]. They found that electrolysis powered by RES, such as wind and solar, offers significant advantages in terms of

GWP per kilogram of hydrogen produced, albeit at the time, its daily production capacity is limited compared to fossil fuel-based methods [67]. Similarly, Dufour et al. analyzed multiple hydrogen production methods, assessing GWP, renewability, and exergy efficiency [68]. Their study found that electrolysis powered by grid electricity has a much higher GWP and performs worse in renewability and exergy efficiency compared to other methods, including SMR with carbon capture [68]. A more recent study by Al-Qahtani et al. evaluated the life cycle impacts of ten hydrogen production pathways, including emerging technologies such as methane pyrolysis, biomass gasification, and PEM electrolysis [69]. By monetizing environmental impact indicators and incorporating them into the total cost, the study found that solar PV-based electrolysis, along with biomass and coal gasification, was among the most expensive technologies due to high capital investment and emission-related costs [69]. Hermesmann and Müller conducted an LCA comparing PEM electrolysis with fossil-based hydrogen production methods across various European locations and technological scenarios [70]. Their results suggest that while PEM electrolysis may become the most environmentally favorable method, its performance is highly sensitive to the electricity mix used in the grid [70].

As electrolysis technologies have become more mature and commercialized over the years, researchers have focused LCA studies on different types of electrolysis technologies. Bareiß et al. performed an LCA of hydrogen production using PEM electrolysis under various energy scenarios and load conditions, showing that integrating PEM electrolysis into energy systems can reduce GWP by at least 30% compared to conventional SMR [71]. Gerloff conducted a comparative LCA on three major electrolysis technologies: alkaline electrolysis, PEM electrolysis, and SOEC, under present and future energy supply scenarios [72]. His assessment found that SOEC has the best environmental performance under fossil dominant energy supply, while PEM electrolysis becomes more favorable as the share of RES increases [72]. A recent study by Iyer et al. also compared the environmental performance of the three major electrolysis technologies under scenarios based in the United States. Their results suggest that PEM electrolysis shows the lowest emissions in stack manufacturing, while SOEC performs best when powered by nuclear energy [73].

Several researchers have also focused their LCA on renewable-based hydrogen production systems. Ghandehariun and Kumar analyzed the life cycle GHG emissions of a wind-powered alkaline electrolysis system in western Canada and reported a 94% reduction in GHG emissions compared to SMR [74]. Burkhardt et al. conducted an LCA on wind-based alkaline electrolysis under a hydrogen FCEV refueling scenario and found that emissions from the storage system of a hydrogen refueling station can account for up to 27% of total life cycle emissions, which is higher than the emissions from electrolyzer manufacturing

[75]. Their study also suggests that operating the electrolyzer at a higher load can lead to lower GHG emissions [75]. Zhang et al. assessed the life cycle impacts of PEM electrolysis and S-I thermal water splitting powered by PV and photothermal (PT) energy sources [76]. They concluded that PEM electrolysis with PV-based supply has the worst environmental performance among the scenarios studied, primarily due to emissions from PV panel construction [76].

Some researchers have coupled LCA with techno-economic studies of green hydrogen systems. Garcia and Oliva conducted a techno-economic study alongside an LCA of Chilean hydrogen production systems powered by both PV and WT, and showed that locations with a greater share of wind energy achieve the lowest life cycle emissions [77]. Al-Ghussain et al. integrated their techno-economic analysis with life cycle emission assessment by formulating a multi-objective optimization that minimizes both the production cost and carbon intensity of a green hydrogen system in California [78]. Their optimized results across different geographic locations suggest that wind-based systems produce consistently low emissions, whereas the carbon intensity of solar-based systems is more inconsistent depending on location [78].

Interest in hydrogen-powered aviation has inspired several LCA studies on the subject. In 2014, Pereira et al. considered the full life cycle of hydrogen-based commercial aviation, including aircraft production and operational emissions within their system boundary, and evaluated the environmental impacts in terms of the cost of emissions from all relevant sources [79]. Their results showed that hydrogen fuel produced via electrolysis powered by RES can achieve a 51% to 60% reduction in environmental costs compared to conventional Jet A fuel [79]. A more recent study by Siddiqui and Dincer compared the life cycle environmental impacts of hydrogen aviation fuel with other alternative fuels such as SAF, also accounting for aircraft manufacturing and operation [80]. Their findings suggest that hydrogen produced via hydropower and geothermal-based electrolysis yields the lowest GWP compared to other pathways, including RES-based electrolysis and SMR [80]. The recent work by Rezaei et al. also examined the environmental performance of the on-site aviation hydrogen production system described in their study, albeit focusing only on the production and delivery components and excluding the RES components. Their work reported a carbon intensity of 0.29 to 0.35 kg CO_2-eq/kg H_2 by 2050 for the hydrogen production and delivery stages [59].

1.3 Motivation and Outline

As mentioned above, there are research gaps in the modeling hydrogen production, storage, supply and refueling infrastructure in an airport at an early implementation stage of hydrogen aviation to understand

their sizing, operation, and potential economic and environmental risks and benefits. Therefore, this thesis complements and extends the existing literature by focusing on the infrastructure design, operational dynamics, economic and environmental impacts of hydrogen infrastructure at early implementation, under conditions of a low or uncertain hydrogen demand. The contribution of this work is the development of a consistent framework for system sizing, techno-economic analysis (TEA) and the LCA of an airport with self-sufficient on-site hydrogen production, storage, liquefaction, and refueling for early implementation of hydrogen-powered commercial flights using data in the Toronto Pearson Airport. The hydrogen infrastructure is powered by both RES and electrical grids. We develop a MILP model to minimize the refueled hydrogen costs with optimal sizes of the system components under different techno-economic scenarios. Historical data on flight schedules at Toronto Pearson Airport and weather data from the Toronto region are used as a case study for this work. This study aims to investigate the optimal design and operation of a renewable-based hydrogen system to support early aviation adopters at airports. It explores the required system capacity, the cost-optimal mix of renewable and grid electricity, and how these parameters evolve over time with changing techno-economic conditions. Additionally, it assesses the life cycle CI of hydrogen production and identifies the key contributors to its environmental impact. This thesis is divided into four chapters. Following the background information and literature review, Chapter 2 focuses on the modeling work of the airport hydrogen system, including the methodology and optimization results. Chapter 3 presents the life cycle assessment (LCA) of the airport hydrogen system, including a description of component life cycle inventories (LCI) and the assessment results. The thesis concludes with a summary of the findings and a discussion on future work and limitations.

Acknowledgement:

Parts of the contents in this chapter are in a manuscript that is under review:

Zhen Ye, Wenrui Ye, John Wen, Xiaoyu. Wu, “Planning renewable hydrogen infrastructure for airports,” Energy, under review, 2025

Chapter 2 Techno-economic Analysis of Airport Hydrogen System

2.1 Introduction

This chapter focuses on the modeling and optimization of a self-sufficient airport hydrogen system. It builds upon the gaps identified in the previous chapter, namely the lack of research addressing small-scale systems designed for the early implementation of hydrogen-based commercial aviation. First, the chapter provides descriptions of all system components involved and outlines the proposed case study. It then presents the formulation of the MILP model used for system optimization. The chapter concludes with a discussion of the optimization results. The key highlights of this chapter aim to address the following questions:

1. What is the capacity of the hydrogen system, including the electrolyzer, liquefaction unit, and storage, required to power early adopters, e.g., regional passenger flights at an airport?
2. What is the share of energy from RES (i.e., PV and WT) and the grid needed to obtain the lowest refueled hydrogen costs?
3. How will the optimal system size change over time based on current and projected techno-economic parameters?
4. How will the integration of RES and grid electricity impact the cost of refueled hydrogen?

2.2 System Description

2.2.1 Energy Supply

The system proposed in this study is illustrated in Figure 2-1, which outlines the general flow of energy between two major components: the electricity supply subsystem and the hydrogen subsystem. Electricity serves as the sole energy source for the entire system. The electricity supply can be sourced from grid electricity, RES, and supplementary batteries, depending on the system configuration. The RES is powered by PV panels, WT or a combination of the two under different scenarios studied in this work. These systems are assumed to be located on the airport premises or in close proximity for on-site hydrogen production and refueling.

The renewable energy production data used in this work is obtained from the open-source renewable generation simulation service provided by Renewable Ninja. This software calculates PV and WT energy

generation using mathematical models developed by Pfenninger and Staffell [81], [82], combined with global weather data from NASA's MERRA database [83]. The Renewable Ninja model assumes that the hourly RES system power output is the product of the hourly RES unit power output and the system capacity.

For the WT system, power output is simulated based on the Enercon E44 900 turbine model in Renewable Ninja. This turbine model was selected under the assumption that its shorter height reduces interference with airport operations when located near the airport. For this case study, the output data for both PV and WT systems is simulated using historic weather data in 2023 from NASA's MERRA database.

In addition, this study assumes that non-renewable energy used by the airport is imported from the public electrical grid, with costs calculated based on the average local electricity price to account of the airports that do not have its own generation microgrid. However, it is known that some large airports may have their own electricity generation facilities and do not draw power from the public grid.

The battery energy storage subsystem (BESS) serves as supplementary storage in this study, providing backup energy to the hydrogen subsystem. The BESS capacity is fixed at 10 MWh and is designed to store electricity from both the grid and renewable sources, particularly during periods when renewable generation exceeds the hydrogen subsystem's energy demand. In this work, we assume that the BESS uses Li-NMC batteries due to their relatively lower cost compared to other lithium battery technologies [84]. The BESS efficiency accounts for the round-trip efficiency, which is 93% for Li-NMC batteries [84]. Detailed techno-economic parameters of the BESS are provided in Table 2-1.

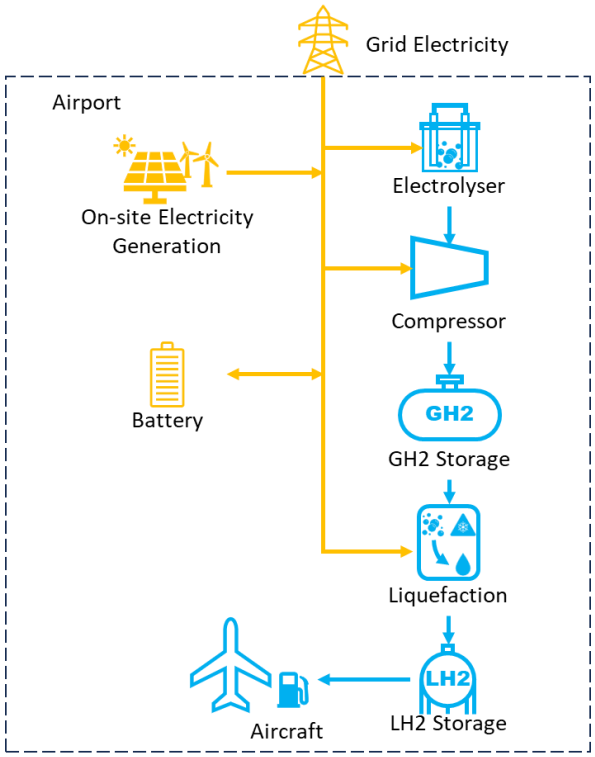


Figure 2-1. Graphical schematic of hydrogen infrastructure in an airport, including on-site hydrogen production using electrolyzers, gas hydrogen (GH2) storage, liquefaction and LH2 storage, and refueling facility. The yellow arrowhead line corresponds to electricity flow and blue arrowhead line corresponds to hydrogen flow.

2.2.2 Hydrogen Subsystem

The hydrogen energy subsystem (HESS) consists of an electrolyzer, GH2 storage, liquefaction units, and LH2 storage. Hydrogen production is carried out by the electrolyzer, which generates GH2 using electricity supplied by the RES and the grid. The electrolyzer technology considered in this work is PEM electrolysis, which offers a faster response to load changes and higher efficiency compared to alkaline electrolysis [18]. The maximum output pressure of a commercially available PEM electrolyzer ranges from 30 to 70 bar [27], [85]. This work adopts a conservative assumption for the output pressure of the PEM electrolyzer, setting it at 30 bar. The techno-economic parameters of the electrolyzer are presented in Table 2-1.

The on-site storage methods were discussed in 1.1.3. This study assumes the same technical basis for GH2 storage methods as presented by Papadias and Ahluwalia [32]. Regarding the storage cost of GH2, aboveground hydrogen storage is considerably more expensive than underground storage due to the cost of tanks [32], [33]. In the base case of this study, GH2 storage is assumed to utilize underground cavern storage due to its economic advantage over aboveground storage. This study also assumes medium-pressure storage at 200 bar for GH2. A compressor is used to pressurize the GH2 from the electrolyzer output at 30 bar to the storage pressure of the cavern storage [30]. For LH2 storage, the study assumes that the tank design geometry and insulation materials are sufficient to maintain cryogenic conditions, as presented in 0. Boil-off losses are accounted for in the system modeling as a percentage of mass lost per hour. The techno-economic details for GH2 storage, LH2 storage, and the compressor are presented in Table 2-1.

The GH2 is liquefied at 1 bar and 23 K using on-site liquefaction units. The ideal minimum specific energy consumption (SEC) for hydrogen liquefaction is 3.9 kWh/kg from the second law of thermodynamics, assuming an inlet condition of 1 bar and 303 K [86], [87]. However, due to efficiency losses in the liquefaction unit components, the actual SEC reported from established industrial plants ranges from 10 to 15 kWh/kg [86], [87]. Future improvements are expected to reduce the SEC of hydrogen liquefaction to 5 to 8 kWh/kg [86], [87]. Regarding liquefaction costs, Holzen et al. reported a non-linear and inverse relationship between the unit cost of liquefaction systems and their size [35]. The cost of small-scale units with a capacity of less than 10 tonne per day (tpd) can exceed 4.5 M USD/tpd of feed, compared to less than 1.5 M USD/tpd for larger plants with capacities exceeding 300 tpd [35]. For this study, as we model early-implementation hydrogen infrastructure, the liquefaction unit is assumed to have a small capacity, estimated based on expected daily fuel demand and available airport space. Under this assumption, the techno-economic parameters for the liquefaction unit in this system are presented in Table 2-1.

2.2.3 Demand

The hydrogen fuel demand is calculated based on historical flight information. In this work, flight data from Toronto Pearson Airport is analyzed to generate a hydrogen fuel demand profile. Based on the aircraft designs announced in Airbus's ZeroE program and the MOU between De Havilland and ZeroAvia [20], it is likely that the initial generation of hydrogen airliners will be powered by fuel-cell-driven engines with specifications comparable to those of the turboprop-powered regional airliners currently in service. For this study, the De Havilland DH-8 series airliner is selected as the reference model to represent a potential hydrogen airliner, as it is reported to be refitted with ZeroAvia's hydrogen engine in the MOU.

Historical flight schedules for services operated by DH-8 series aircraft from Toronto Pearson Airport in February 2024 are collected from the open-source flight information website FlightRadar24 [88]. This data is used to create an hourly hydrogen demand schedule as follows. First, the flight history for each destination is analyzed to determine the average flight time of trips. This information is then used to estimate kerosene fuel consumption for each flight, which will be converted to hydrogen consumption for flights to each destination using the conversion factors for substituting LH2 for kerosene jet fuel across various aircraft sizes reported in [47]. Lastly, the resulting data is constructed in an hourly hydrogen demand profile derived from flight schedules, as shown in Figure 2-2.

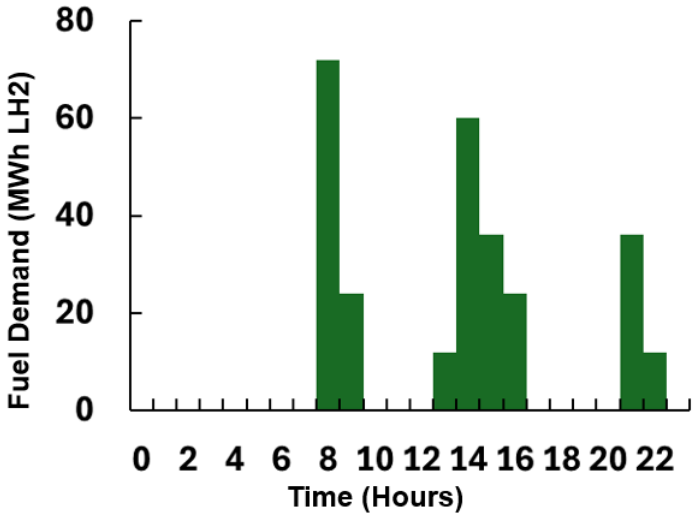


Figure 2-2. Fuel demand schedule of the Toronto Pearson Airport case-study

Table 2-1. 2025 Base Case techno-economic parameters of the system components. The numbers in parentheses indicate the techno-economic predictions for the 2050 Case.

Component	Unit	CAPEX	Fixed OPEX	Efficiency	SEC ($kWh/kg\ H_2$)	Loss (% mass/hr)	Note
PV	$/kW	650 (400)	1.3%	-	-	-	a
WT	$/kW	1300 (1000)	1.1%	-	-	-	a
Electrolyzer	$/kW	1000 (300)	3.0%	70% (75%)	-	-	b
GH2 Storage	$/kg	20 (20)	1.5%	-	-	-	c
LH2 Storage	$/kg	55 (25)	2.0%	-	-	0.1%	d
Liquefaction	M US$/tpd	5.5 (3.5)	4.0%		13 (8)	0.2%	e
Battery	$/kWh	250 (120)	3.0%	93%	-	-	f
Compressor	$/kW	1000 (600)	4.0%	-	0.82 (0.84)	0.5% (0.4%)	g

a. The unit CAPEX values of PV and WT components are derived from the reported values in references [89], [90], and the fixed OPEX values are calculated based on the reported values in [60], [89], [90].
b. The unit CAPEX of the electrolyzer technology, along with future cost projections, is reported in several references [31], [35], [89], [90], [91], [92]. The unit CAPEX value used in this work is derived from the values collected from these sources. The efficiency of PEM electrolyzer technology is reported in [31], [89], [91]
c. The techno-economic parameters of the bulk GH2 storage unit in this work are taken from references [31], [32], [47].
d. The techno-economic parameters of the LH2 storage unit are taken from [30], [47]
e. The economic parameters of the liquefaction unit are taken from [30], [35]. The technical parameter SEC value for liquefaction technology is derived from reported values in [86], [93].
f. The battery efficiency considers the round-trip efficiency and is reported in [84]. The techno-economic parameters of the battery system are adapted from [94], [95].
g. The techno-economic parameters of the compressor component in the system are taken from a report by the U.S. Department of Energy [30].

2.2.4 Case Studies

Multiple case studies are conducted to investigate the cost-benefits of system configuration variations and techno-economic advancements on optimized system sizing. Table 2-2 summarizes the case studies and highlights their configurations. The 2025 Base Case is established with both grid-connected energy supply and RES, composed of PV and WT, using techno-economic data from 2025. The Base Case serves as the benchmark scenario for assessing the performance of the MILP model and examining detailed system performance. System configuration cases with 100% RES are analyzed using the 2025 techno-economic parameters to evaluate the feasibility of a renewable hydrogen infrastructure at an airport. These cases include PV-Only, WT-Only, and RE-Only configurations; the last one combines PV and WT for electricity input. The grid-connected 2050 Case is developed using predicted techno-economic parameters for 2050 and is compared to the Base Case to investigate the impacts of technological development and market expansion on the optimization results.

Table 2-2. Summary of case study configurations used in this work.

Case Studies	Grid	PV	WT	Parameter Year
Base Case	✓	✓	✓	2025
RE Only		✓	✓	2025
WT Only			✓	2025
PV Only		✓		2025
2050 Case	✓	✓	✓	2050

2.3 Methodology

This work employs a MILP model to determine the optimal component configuration of the airport hydrogen infrastructure by minimizing the overall annualized cost while satisfying constraints derived from the system's energy balance. For modeling hydrogen systems, linear modeling in the form of LP or MILP is a popular choice of method in the literature, which provides reasonable representation of the system's complexity while ensuring its computability. MILP methods have been used in the studies on hydrogen airport systems [47], hydrogen supply chain problems [35], [49], [50], [52], [55], [96] and hydrogen storage systems in microgrids [60], [61], [62], [63]

The inputs to the MILP model include the RES generation profile, the hydrogen demand profile at the airport, and the techno-economic parameters of all the components in the system outlined in Table 2-1. Figure 2-3 provides a graphical representation of the detailed energy flow within the system, from

electricity generation by RES to hydrogen consumption by aircraft. The mathematical expressions for the constraints will be detailed in the following sections. These constraints ensure that the hydrogen demand from flights is met at all time steps while the demand and supply of each system component remain within their respective capacities. The decision variables of the MILP model include the capacities of the system components, and the amounts of grid electricity purchased. The MILP model optimizes the decision variables while simultaneously managing the system's energy flow at each time step of the simulation. For this study, the time step is set to be one hour.

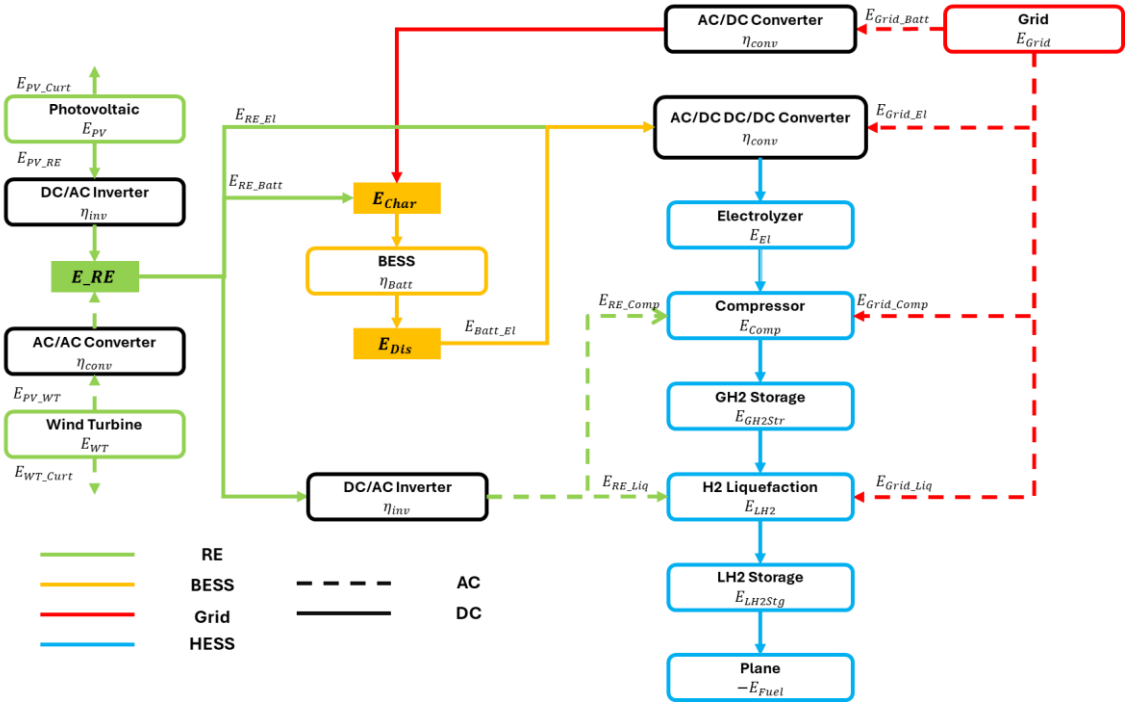


Figure 2-3. Detailed schematic of energy flow within the airport hydrogen system. The dashed arrowhead line corresponds to flow of AC energy while the solid arrowhead line corresponds to flow of DC energy. The color scheme highlights different subsystems with green corresponding to RES subsystem, yellow corresponding to battery storage, blue corresponding to hydrogen subsystem and red represents grid energy.

2.3.1 Objective Function

The objective function of the MILP model is minimizing the total expenditure of the system,

$$\min (C_{Grid} + \sum_{j} C_{T,A,j}) \quad \textbf{Equation 2-1}$$

Where C_{Grid} is the cost of grid electricity used in a year which is represented in Equation 2-2, and $C_{T,A,j}$ is the annualized total expenditure of system component j, represented in Equation 2-3. Here j represents the components in the airport hydrogen system, including PV subsystem, WT subsystem, electrolyzer, liquefaction unit, compressor, gaseous storage and liquid storage.

The yearly grid energy purchase cost C_{Grid} is calculated as the product of unit cost of grid electricity imported to the system, $C^{U}_{Grid,i}$, and the sum of grid electricity purchased, $E_{Grid,i}$, at time i in hours, as

$$C_{Grid} = C^{U}_{Grid,i} * \sum_{i} E_{Grid,i} \quad \textbf{Equation 2-2}$$

The annualized total expenditure of a component, $C_{T,A,j}$, is calculated using Equation 2-3, the product of the component capacity, CAP_j and the annualized component unit cost $C^{U}_{T,A,j}$.

$$C_{T,A,j} = C^{U}_{T,A,j} * CAP_j \quad \textbf{Equation 2-3}$$

The annualized component unit cost $C^{U}_{T,A,j}$ in Equation 2-3 considers the annualized unit capital expenditure, $C^{U}_{C,A,j}$ and its fixed operating expenditure, $C^{U}_{FO,j}$ (as see in Equation 2-4).

$$C^{U}_{T,A,j} = C^{U}_{C,A,j} + C^{U}_{FO,j} \quad \textbf{Equation 2-4}$$

The annualized capital expenditure, $C^{U}_{C,A,j}$, can be calculated by multiplying the unit capital expenditure $C^{U}_{C,j}$ listed in Table 2-1 by the capital recovery factor, f_{CR}, as

$$C^{U}_{C,A,j} = C^{U}_{C,j} * f_{CR} \quad \textbf{Equation 2-5}$$

Since the units of $C^{U}_{C,j}$ in Table 1 vary between different components (i.e. US$/kW for WT and US$/kg for GH2 storage), the units of these parameters are all converted to equivalent units in power or energy, i.e., US$/kW for power consuming and power generating components, US$/kWh for storage components. Correspondingly, the units of component capacity CAP_j depend on the type of component its representing.

The capital recovery factor f_{CR} is a ratio used to calculate the annualized cost of an investment, considering the time value of money. f_{CR} is calculated using annual discount rate and project lifetime,

$$f_{CR} = \frac{dr(1+dr)^{LT}}{(1+dr)^{LT}-1} \quad \textbf{Equation 2-6}$$

where, dr represents the annual discount rate, i.e., 0.07 in this study, and LT is the project lifetime, i.e., 20 years in this study.

In this study, the fixed operating cost of component j, $C^{U}_{FO,j}$, is assumed to be a fixed percentage of its $C^{U}_{C,j}$ every year. The percentage value is represented by the factor $f_{FO,j}$, which is listed in Table 2-1.

$$C^{U}_{FO,j} = C^{U}_{C,j} * f_{FO,j} \quad \textbf{Equation 2-7}$$

2.3.2 Electricity Supply Constraints

The following equations outline a set of constraints for the energy balance of electricity supply from RES and grid to the system.

$$\dot{E}_{PV,i} * CAP_{PV} * dt = E_{PV_RE,i} + E_{PV_curt,i} \quad \textbf{Equation 2-8}$$

$$\dot{E}_{WT,i} * CAP_{WT} * dt = E_{WT_RE,i} + E_{WT_curt,i} \quad \textbf{Equation 2-9}$$

Equation 2-8 and Equation 2-9 ensure that the production and curtailment of renewable energy are constrained by the RES component capacity and the RES production profile of the case-study region. $\dot{E}_{PV,i}$ and $\dot{E}_{WT,i}$ are inputs from Renewable Ninja (see 2.2.1), which describes the power generation by PV and WT per unit capacity of the components, respectively.

Meanwhile, the utilized renewable energy, $E_{RE,i}$ and the purchase of grid energy, $E_{Grid,i}$ are constrained in Equation 2-9, Equation 2-10 and Equation 2-11by consumption of energy supply by the battery storage and the hydrogen systems. The variables in the equations are shown in Figure 2-3.

$$E_{RE,i} = E_{PV_RE,i} * \eta_{Inv} + E_{WT_RE,i} * \eta_{Conv} \quad \textbf{Equation 2-10}$$

$$E_{RE,i} = E_{RE_Batt,i} + E_{RE_El,i} + E_{RE_Liq,i} + E_{RE_Comp,i} \quad \textbf{Equation 2-11}$$

$$E_{Grid,i} = E_{Grid_Batt,i} + E_{Grid_El,i} + E_{Grid_Liq,i} + E_{Grid_Comp,i}$$ **Equation 2-12**

2.3.3 Battery System Constraints

Equation 2-13 and Equation 2-14 describe the battery charging $E_{Char,i}$ and discharging $E_{Dis,i}$ at each time step, respectively. $E_{Char,i}$ consists of the energy supplied from the RES and the grid, with losses introduced by converter efficiency and the roundtrip battery losses.

$$E_{Char,i} = \left(E_{RE_Batt,i} + E_{Grid_Batt,i}\right) * \eta_{Conv} * \eta_{Batt}$$ **Equation 2-13**

$$E_{Dis,i} = E_{Batt_El,i}$$ **Equation 2-14**

Meanwhile, the energy stored inside the battery storage, $E_{Batt,i}$, at the beginning time step, i = 0 is specified,

$$E_{Batt,i=0} = E_{Batt_init}$$ **Equation 2-15**

The energy balance of the battery is as,

$$E_{Batt,i} = E_{Batt,i-1} + E_{Char,i-1} - E_{Dis,i-1}$$ **Equation 2-16**

The imposed constraints in Equation 2-17 to Equation 2-19 ensure that the battery system will not perform charging and discharging at the same time. Here, B_{Dis} and B_{Char} are the binary integer that enforce the constraints and M denote the constant with an arbitrary high value.

$$M * B_{Char} \leq E_{Char,i} \leq M * (1 - B_{Dis})$$ **Equation 2-17**

$$M * B_{Dis} \leq E_{Dis,i} \leq M * (1 - B_{Char})$$ **Equation 2-18**

$$B_{Dis} + B_{Char} = 1$$ **Equation 2-19**

2.3.4 Gaseous Hydrogen System Constraints

Equation 2-20 describes the energy balance at the electrolyzer, where the energy consumption by the electrolyzer is constrained by the energy supplied from the RES, the battery storage, and the grid.

$$E_{El,i} = E_{RE_El,i} * \eta_{Conv} + E_{Batt_El,i} * \eta_{Inv} + E_{Grid_El,i} * \eta_{Conv}$$ **Equation 2-20**

The electric energy demand from the electrolyzer is lower or equal to the capacity of the electrolyzer, CAP_{El}, as is shown in Equation 2-21.

$$E_{El,i} \leq CAP_{El} * dt$$ **Equation 2-21**

The storage level of GH2 at time i is equal to the level at the previous time step, $i-1$, plus the generated hydrogen at time i, and subtracting the GH2 drawn by the liquefaction system (as seen Equation 2-22).

$$E_{GH2Stg,i} = E_{GH2Stg,i-1} + E_{El,i-1} * \eta_{El} * \eta_{Comp} - E_{LH2,i-1}$$ **Equation 2-22**

The generated hydrogen at each time i is calculated as the electricity power consumption by the electrolyzer $E_{El,i}$ multiply by the efficiency of the electrolyzer, η_{El} and the compressor efficiency, η_{Comp}.

Equation 2-23 imposes additional constraints on the storage level to ensure that the level is below maximum storage capacity. The minimum storage level of GH2 is also constrained to 10% of the maximum storage capacity to prevent pressure instability.

$$0.1 * CAP_{GH2Stg} \leq E_{GH2Stg,i} \leq CAP_{GH2Stg}$$ **Equation 2-23**

And the storage level at the end of simulation needs to be higher than the initial value to ensure a sustainable operation.

$$E_{GH2Stg,i=0} \leq E_{GH2Stg,i=End}$$ **Equation 2-24**

Equation 2-25 and Equation 2-26 describe the energy balances at the compressor. First, the energy consumption by the compressor, $E_{Comp,i}$, is calculated based on the generated hydrogen at each time i and the specific energy consumption of the compressor, SEC_{Comp}.

$$E_{Comp,i} = E_{El,i} * \eta_{El} * SEC_{Comp}$$ **Equation 2-25**

And compressor's energy demand is from the grid and RES, as

$$E_{Comp,i} = (E_{Grid_Comp,i} + E_{RE_Comp,i}) * \eta_{Inv}$$ **Equation 2-26**

The compressor capacity, CAP_{Comp}, is related to the electrolyzer capacity, CAP_{El}, ensuring sufficient compression for the hydrogen output from the electrolyzer (see Equation 2-27).

$$CAP_{Comp} = CAP_{El} * \eta_{El} * SEC_{Comp}$$ **Equation 2-27**

2.3.5 Liquid Hydrogen System Constraints

The equations in this section represent the constraint for LH2 system, which involves the energy balance in the liquefaction unit, liquid state storage and the ultimate fuel demand from the aircraft, as

$$SEC_{Liq} * E_{LH2,i} = (E_{RE_Liq,i} + E_{Grid_Liq,i}) * \eta_{Inv}$$ **Equation 2-28**

Here, the energy consumption by the liquefaction unit is calculated by multiplying the specific energy consumption of the liquefaction unit SEC_{Liq} and the amount of liquefied hydrogen $E_{LH2,i}$.

Yet, $E_{LH2,i}$ is constrained by the capacity of liquefaction unit, as

$$E_{LH2,i} \leq CAP_{Liq} * dt$$ **Equation 2-29**

The storage level of LH2 at time i, $E_{LH2Stg,i}$, is calculated similarly to the gaseous storage, which equals to the level of the previous time step $i-1$, plus the liquefied hydrogen and subtracting the fuel delivered to the aircraft, as

$$E_{LH2Stg,i} = E_{LH2Stg,i-1} * (1 - \eta_{LH2}) + E_{LH2,i-1} * \eta_{Liq} - E_{Fuel,i-1}$$ **Equation 2-30**

Here, an additional loss efficiency η_{LH2} is added to the storage level balance for LH2 storage to address the boil-off losses.

Similar to GH2 storage, additional constraints are imposed on the storage level of LH2 to ensure sustainable operation (Equation 2-31) and that the level is bounded within the storage capacity and minimal operation capacity (Equation 2-32).

$$E_{LH2Stg,i=0} \leq E_{LH2Stg,i=End}$$ **Equation 2-31**

$$0.1 * CAP_{LH2Stg} \leq E_{LH2Stg,i} \leq CAP_{LH2Stg}$$ **Equation 2-32**

2.3.6 Performance Indicators

The levelized cost of hydrogen (LCOH) is a useful indicator of the cost-effectiveness of a hydrogen production system. It represents the cost of producing hydrogen on a per-unit basis. In this study, the LCOH is calculated using the annualized total cost of the system, which includes the cost of the battery system, and the yearly LH2 production in kilograms, as shown below.

$$LCOH = \frac{C_{Grid} + \sum_j C_{T,A,j}}{\sum_i E_{El,i} * \eta_{El} * \eta_{Comp}}$$ **Equation 2-33**

Several technical indicators are introduced to evaluate the overall performance of the system and the individual performance of specific system components. The energy independence score (EIS) evaluates the degree of system's energy independence from conventional grid energy [97].

$$EIS = 1 - \frac{\sum_{i=1}^{t} E_{Import,i}}{\sum_{i=1}^{t}(E_{Import,i} + E_{RE,i})}$$ **Equation 2-34**

On the component level performance, the utilization ratio (or capacity factor) of electrolyzer, U_E, and liquefaction unit, U_L, are calculated as the average ratio of the actual utilized capacity over its maximum capacity.

$$U_E = \frac{\sum_{i=1}^{t} \frac{E_{ElDemand,i}}{CAP_{j=El}}}{t}$$ **Equation 2-35**

$$U_L = \frac{\sum_{i=1}^{t} \frac{E_{LiqDemand,i}}{CAP_{j=El}}}{t}$$ **Equation 2-36**

The curtailment ratio of renewable energy, R_C, is calculated as the average summation of curtailed PV and WT energy, over the total renewable generation.

$$R_C = \frac{\sum_{i=1}^{t}(E_{WT_Curt,i} + E_{PV_Curt,i})}{\sum_{i=1}^{t} E_{RE,i}}$$ **Equation 2-37**

2.4 Results and Discussion

2.4.1 2025 Base Case

2.4.1.1 System Performance and Optimization

In the 2025 Base Case, hydrogen infrastructure in the airport is powered by both grid electricity and RES comprised of PV and WT with techno-economic parameters in 2025. Results of the base case study will be used to examine the system operation performance and serve as the baseline for comparison with other case studies and sensitivity analysis. A summary of all the cases can be found in 2.2.4.

The optimized component capacities and their costs for the 2025 Base Case are presented in Table 2-3. The total annualized system cost is US$ 19.6M, with an additional cost of US$ 3.4M for grid electricity. It is notable that despite having a rather low capacity, the cost of the liquefaction unit takes up 31.2% of the overall expenditure, due to its particularly high cost per unit capacity.

The LCOH of the 2025 Base Case is US$7.45/kg LH2. This value is higher than the US$5.38/kg plant-gate cost reported by the US Department of Energy [98]. However, it is significantly lower than the cost of the dispenser in their study, i.e., US$14.24/kg [98], because the on-site hydrogen infrastructure in this study does not require costly distribution and retail. This value is also compared to values from the literature under similar scenarios. Schenke et al. reported an LCOH of US$5.3 to US$13.3/kg LH_2 in their study on on-site LH_2 production for the early adoption of hydrogen aviation in 2030, across different European locations and flight numbers [58]. In comparison, the result obtained in our study lies within the middle of the range reported by Schenke et al., supporting the assumptions made in this study and indicating consistency in system performance across scenarios from different locations.

Compared to fuel prices, over the past five years the daily jet fuel spot price reported by the U.S. Energy Information Administration (EIA) has ranged from US$0.29/kg to US$1.73/kg [99] (*Note: the lower end of this range occurred during the COVID-19 period and may not reflect typical market conditions*), it still costs significantly less by unit fuel weight using jet fuels than using LH2. For an alternative perspective, the costs of both hydrogen and jet fuel are converted to a per-kWh basis. Under this metric, the LCOH is US$0.22/kWh for LH_2, while the costs of jet fuel remain lower at US$0.024/kWh to US$0.14 US$/kWh, making hydrogen under the 2025 Base Case still less competitive than its jet fuel counterpart.

Table 2-3, Summary and comparison of simulation results for the 2025 Base Case, RE Only, PV Only, WT Only cases and 2050 Case. The top section of the table summarizes the results for system component capacities; the middle section shows the overall system cost and the breakdown of system component costs; and the bottom section presents the technical indicators for case study performance assessment.

	Base Case	RE Only	PV Only	WT Only	2050 Case
PV	51.47 MW	63.82 MW	214.02 MW	-	72.8 MW
WT	42.59 MW	56.2 MW	-	107.71 MW	33.1 MW
Electrolyzer	28.31 MW	36.44 MW	50.48 MW	41.85 MW	42.75 MW
Liquefaction	10.23 tpd	9.51 tpd	32.48 tpd	13.34 tpd	10.23 tpd
Compressor	0.49 MW	0.63 MW	0.87 MW	0.72 MW	0.81 MW
LH2 Storage	3.42 t	24.63 t	26.92 t	36.81 t	3.42 t
GH2 Storage	28.64 t	222.94 t	522.29 t	683.94 t	210.69 t
Battery Storage	10 MWh	10 MWh	10 MWh	10 MWh	10 MWh
Grid Energy	38.61 GWh	-	-	-	0.97 GWh
PV	$3.3 M	$4.1 M	$13.9 M	-	$2.9 M
WT	$5.4 M	$7.1 M	-	$13.6 M	$3.2 M
Electrolyzer	$3.3 M	$4.2 M	$5.9 M	$4.9 M	$1.5 M
Liquefaction	$7.2 M	$6.7 M	$22.7 M	$9.3 M	$4.5 M
Compressor	$61.5 K	$79.1 K	$109.6 K	$90.9 K	$61 K
LH2 Storage	$19.7 K	$142.2 K	$155.5 K	$212.6 K	$10 K
GH2 Storage	$52 K	$404.6 K	$948 K	$1.2 M	$382 K
Battery Storage	$290 K	$290 K	$290 K	$290 K	$140 K
Grid Energy	$3.4 M	-	-	-	$10 K
System Total	$22.9 M	$22.9 M	$43.8 M	$29.6 M	$12.8 M
ELE Utilization	58.79%	45.63%	34.07%	41.72%	36.31%
LIQ Utilization	81.71%	88.18%	26.58%	65.69%	81.73%
% Curtailment	7.90%	9.30%	31.20%	15.20%	4.20%
EIS	0.80	-	-	-	0.99

2.4.1.2 Operation Performance



Figure 2-4, Simulation results for 2025 Base Case; a) Annual energy supply breakdown; b) Hourly energy supply dynamics during moderate renewable availability; c) Hourly energy supply dynamics during high renewable availability; d) Daily energy supply dynamics; e) Weekly energy supply percentage; f) Renewable energy utilization dynamics.

Figure 2-4 provides a detailed breakdown of energy sources for the airport hydrogen system throughout the year in the 2025 Base Case. Figure 2-4 a) shows the annual energy supply proportion of different sources. Figure 2-4 a) reveals that renewable energy supplies the majority of the electrolyzer's energy over the year in the 2025 Base Case, with PV and WT providing 20% and 50% of the system's annual energy supply, respectively. Figure 2-4 b) and c) depict two four-day hourly profiles of the electrolyzer energy supply during moderate (e.g., Days 0-3) and high renewable availability (e.g., Days 62-65), respectively. In periods with moderate renewable availability (see Figure 2-4 b)), renewable energy alone cannot meet the power demand from the electrolyzer, so grid energy fills the gap to ensure a steady hydrogen supply for flights. On the other hand, under high renewable availability, the system can operate solely on renewable sources. Figure 2-4 c) also shows that periods of low energy consumption by the system occur during seasons of high renewable energy availability. This suggests that the system chooses to slow down hydrogen production and instead utilizes stored hydrogen during periods of overproduction to meet fuel requirements. This highlights the important role of hydrogen storage in energy management, enabling the system to operate with greater flexibility and improved utilization of renewable energy.

Figure 2-4 d) shows the daily source energy breakdown for the entire year, while Figure 2-4 e) presents the weekly percentage contribution of each energy source powering the electrolyzer. Moreover, Figure 2-4 f) provided the details of renewable energy generation in the system throughout the year. During the winter and spring seasons between Weeks 4 and 16 (Figure 2-4 e)) or Days 28 to 112 (Figure 2-4 f)), abundant wind energy is available in the local area. This corresponds to the high renewable availability days when the system operates solely in RES, as discussed before.

2.4.1.3 Sensitivity Analysis

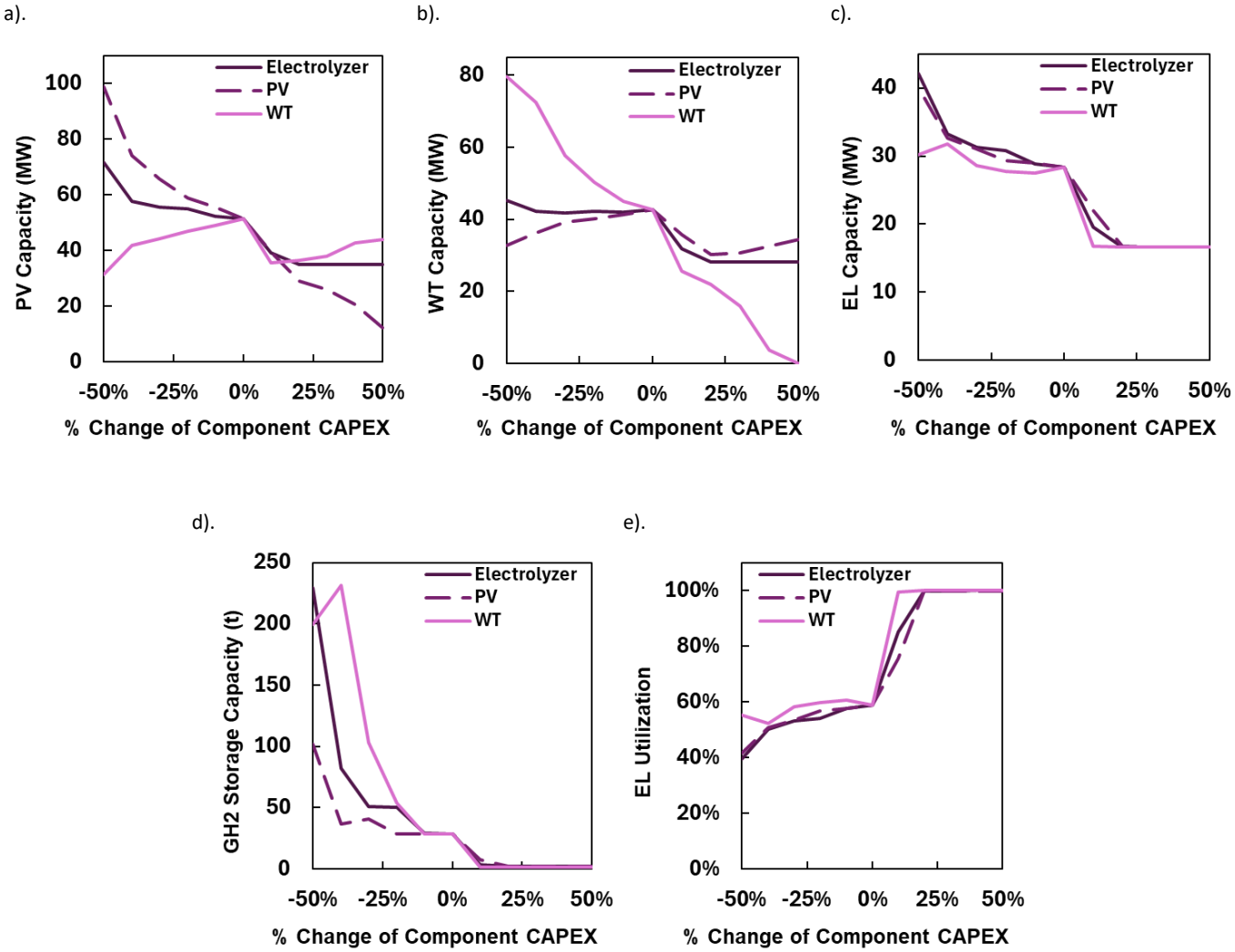


Figure 2-5. Impact of change in unit CAPEX of PV, WT and electrolyzer on the results of a). PV sizing, b). WT sizing, c). Electrolyzer sizing, d). GH2 Storage sizing, and e). Electrolyzer utilization.

Market fluctuations, component availability and supply chain, and technology improvement may all impact the price of subcomponents in the system. To examine how these could affect the sizing and economic performance of the hydrogen system, sensitivity analysis is performed with varying unit costs for PV, WT, and electrolyzers. It is noted that during these sensitivity analyses, the sizing for the liquefaction unit and LH2 storage remain unaffected due to their high unit costs and specific energy

consumption of the liquefaction component (as seen in Table B 1). The impacts on the sizing and economic results of various components are plotted in Figure 2-5 and Figure 2-6, respectively.

Figure 2-5 a) depicts how the changes in the PV, WT and electrolyzer costs impact on the sizing of PV system capacity. The change in electrolyzer and PV unit costs affect the PV system capacities similarly; namely, both unit costs correlate inversely with the optimized PV capacities. On the other hand, a decrease in the unit cost of WT reduces PV system capacity, as WT becomes more cost-effective compared to PV. However, when WT costs increase by more than 10%, PV capacity starts to rise as the cost of PV energy becomes significantly cheaper than the cost of WT energy, making a larger PV capacity more beneficial for providing renewable energy.

The impacts on the WT capacity sizing are shown in Figure 2-5 b). The optimized capacity of WT is inversely correlated with changes in the unit costs of both WT and electrolyzer components. While WT capacity is not highly sensitive to reductions in electrolyzer costs, it is significantly affected by changes in WT costs. If the unit cost of WT increases by more than 50%, optimized configuration indicates that incorporating a WT component would no longer be economically viable and thus the size of WT at this point reduces to zero. Additionally, WT capacity decreases as PV costs decline; and once PV costs rise beyond 20%, WT capacity begins to increase. This trend is similar to the observations made for the impact of WT cost on PV capacity in Figure 2-5 a), suggesting that changes in the cost of one renewable technology can similarly impact the capacity of the other.

The sizes of the electrolyzer module and GH2 storage are similarly sensitive to changes in the unit costs of PV and electrolyzers, as shown in Figure 2-5 c) and d). And GH2 storage size becomes particularly sensitive when these costs decrease by more than 40%. From Figure 2-5 a) to d), it also indicates that once the electrolyzer unit costs increase by more than 10%, these component capacities are not significantly affected by increases in electrolyzer unit costs anymore. That’s because when electrolyzer unit costs are high, it becomes financially optimal to only use the smallest possible electrolyzer. Under such a configuration, the system's operation strategy shifts drastically, as the electrolyzer is at full capacity, i.e., its utilization caps at 100% as shown in Figure 2-5 e). This means that the system requires nonstop hydrogen production to meet the daily hydrogen consumption from flights.

Impacts of component unit costs on financial performance are reflected in the variation of LCOH, as shown in Figure 2-6 a). Generally, LCOH is directly related to changes in the unit costs of component technologies, showing greater sensitivity to cost reductions than to cost increases. Notably, LCOH is

particularly responsive to decreases in WT technology costs, with a 50% reduction in WT cost leading to a 16% drop in LCOH. Additionally, Figure 2-6 b) and c) illustrate the sensitivity of component expenditure and grid energy purchases to component technology unit costs, respectively. Component expenditure remains relatively stable with cost reductions of up to 40%, because component sizes increase with unit cost reduction. But grid energy purchases directly correlate with changes in component costs, as shown in Figure 2-6 c). This is due to the corresponding decrease in component capacities, as shown earlier in Figure 2-5. As component costs rise, operating the hydrogen system using renewable energy becomes very expensive, leading the system to increase the reliance on grid energy to compensate for energy availability constraints (as also seen in the EIS changes in Table B 1).

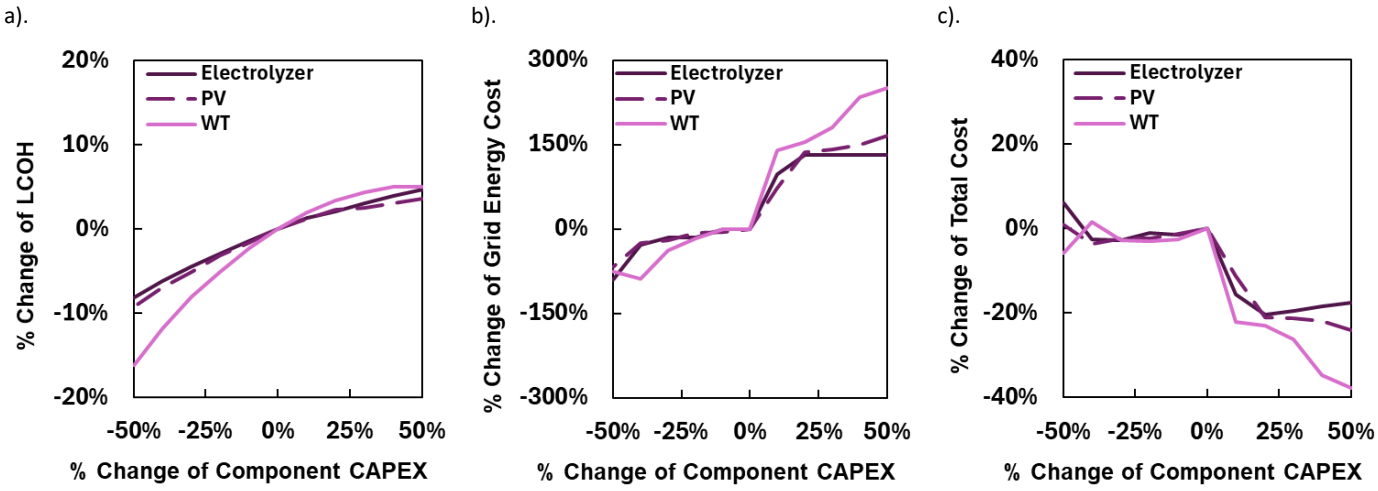


Figure 2-6. Impact of change in unit CAPEX of PV, WT and electrolyzer on the economic results of a). Total annualized component expenditure, b). Annual grid energy cost, and c). LCOH.

The impact of electrolyzer efficiency is also analyzed. We consider the efficiency range of 50% to 80% to cover both the pessimistic performance of current technology and the optimistic performance of future targets. Figure 2-7 illustrates that improvements in electrolyzer efficiency can significantly reduce the overall cost of the system. The total system cost can be reduced by 7% compared to the current value from the 2025 Base Case. A more efficient electrolyzer also decreases energy demand, leading to a reduction in the capacities of the renewable energy grids (see Figure 2-7 b)). The PV and WT sizes are reduced by 9.6% and 10.4%, respectively, if electrolyzer efficiency is improved to 80%. In Figure 2-7 c) and d), changes in efficiency in both directions result in a slight decrease (less than

7%) in the required GH2 storage and a small increase (less than 2%) in electrolyzer utilization, indicating that variations in electrolyzer efficiency do not significantly impact the storage requirements or operational demand of the system.

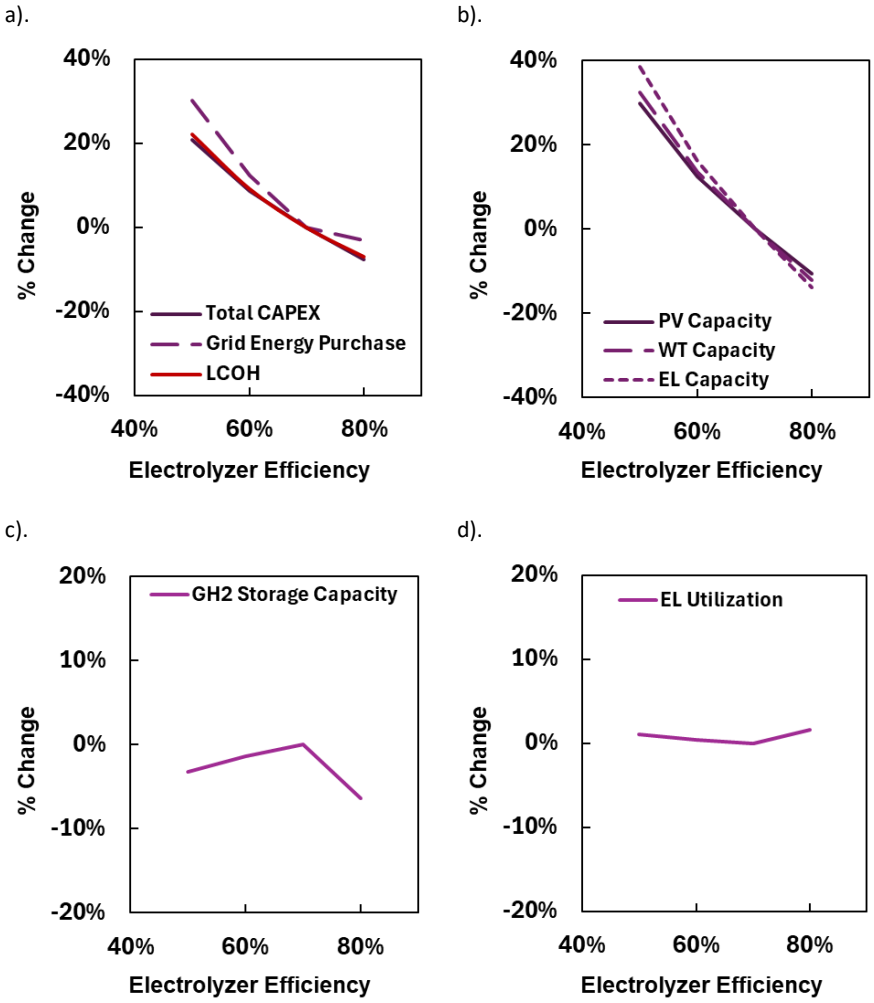


Figure 2-7. Impact of electrolyzer efficiency on the optimal results, a). System economics performance; b). Renewable and Electrolyzer system sizing; c). GH2 Storage sizing; d). Electrolyzer utilization.

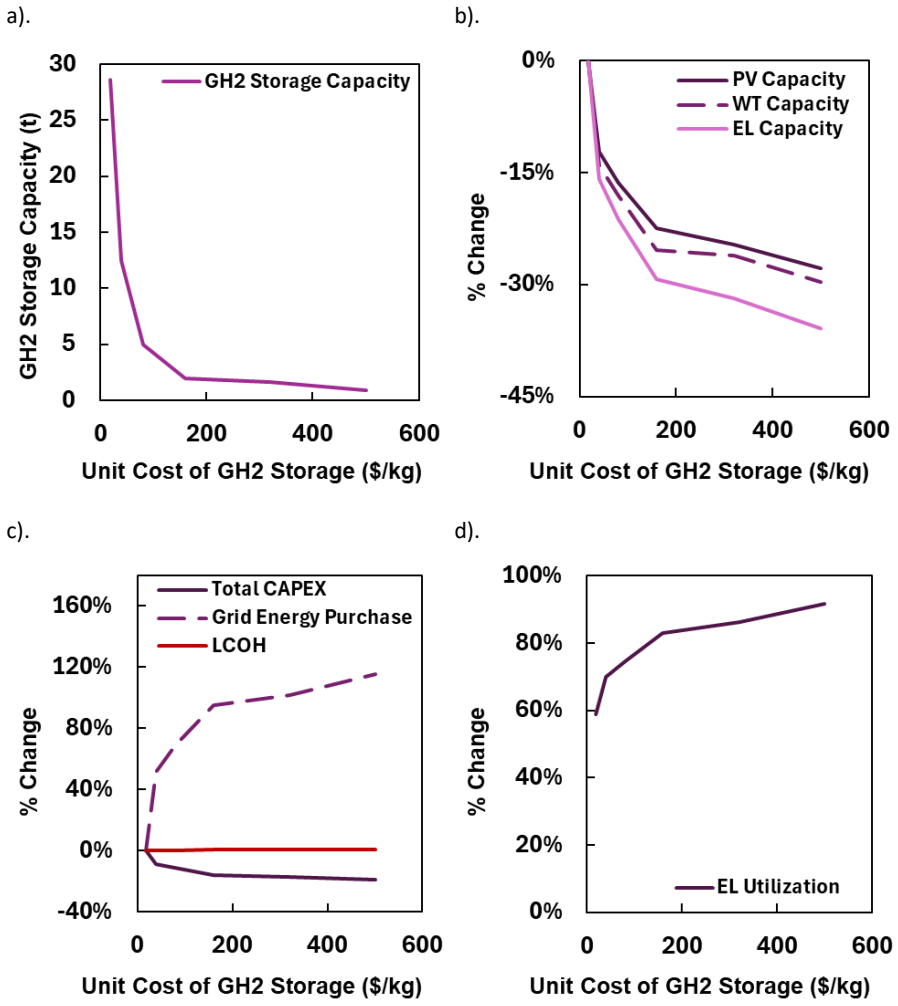


Figure 2-8. Impact of unit cost of GH2 storage on the optimal results, a). GH2 Storage sizing; b). Renewable and Electrolyzer system sizing; c). System economics performance; d). Electrolyzer utilization.

The 2025 Base Case assumes that the GH2 is in cavern storage as a cheap method to store bulk hydrogen in gaseous state. However, the cost of cavern storage for GH2 can vary due to the location and costs of labour and construction [32]. In cases where cavern storage may not be available, compressed storage tanks will be adopted for potential GH2 storage. For these reasons, sensitivity analysis on the unit cost of GH2 storage to the sizing results is conducted to investigate the effect of the varying storage situations. In this study, a range between the unit cost of cavern storage cost (i.e., US$20/kg [35]) and

the unit cost of compressed gas tank storage (i.e., US$500/kg [30]) is analyzed. Figure 2-8 a) and b) show that the optimized component sizes are inversely related and highly sensitive to increases in storage costs. A sharp decrease in GH2 storage size is observed as its costs rise from US$20/kg to US$200/kg, leading to a corresponding reduction in renewable energy and electrolyzer component sizes. Despite this, the system's overall economic performance remains unaffected, with the LCOH staying nearly the same by adjusting the use of RES and grid electricity to produce hydrogen, as is shown in Figure 2-8 c). Nonetheless, higher GH2 storage costs alter the system's component size composition and reduce the system's potential to produce hydrogen using renewable energy as the grid reliance increases (as also seen in the EIS changes in Table B 1). In addition, Figure 2-8 d) shows that higher GH2 storage costs may also impact the system's operating pattern, as electrolyzer utilization increases significantly with rising GH2 storage costs.

2.4.2 Case Studies

2.4.2.1 Without grid connections

The PV-Only, WT-Only, and RE-Only case studies are conducted to evaluate the economic and technical feasibility of setting up the airport hydrogen infrastructure without grid-connection (see 2.2.4). Table 2-3 compares system component capacities, annualized costs, and technical performance among all case studies.

Figure 2-9 illustrates the contribution of component costs to the LCOH. It shows that producing hydrogen using only one type of renewable technology is very costly due to significant increase in the required production, liquefaction and storage capacities. The total costs for the PV-Only and WT-Only cases are 90.9% and 29.0% higher, respectively, than that for the Base Case grid-connected system. Although the total renewable subsystems cost similarly in the PV-Only case (US$13.9 M) and the WT-Only case (US$13.6 M), the PV-Only case has a much more expensive hydrogen subsystem including both electrolyzer and liquefaction unit. In the PV-Only case, the hydrogen subsystem cost is US$29.8 M accounting for 68.0% of the total cost, while for the WT-Only scenario, it costs US$15.7 M, representing only 53.2% of the total cost. The high expense of the PV-Only configuration is due to the limited availability of PV during the daytime and the large seasonal variation in sunlight from the historic weather data near Toronto. This restricts hydrogen production in the PV-Only configuration to

daytime, resulting in the need for a much larger electrolyzer and liquefaction unit working in a shorter window to meet the fuel demand. Additionally, the system requires larger storage capacity to accommodate large seasonal PV generation changes.

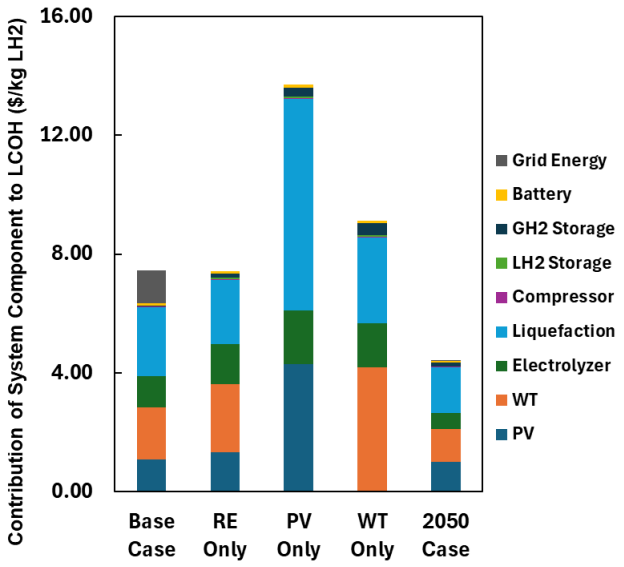


Figure 2-9. Contribution of system component cost to LCOH for 2025 Base Case, RE-Only, PV-Only, WT-Only and 2050 Case.

In contrast, the total annualized cost of the RE-Only case is only 0.13% higher than the Base Case with grid connection, making it much cheaper than the PV-Only and WT-Only scenarios. This is because the RE-Only case benefits from the strengths of both PV and WT technologies, with PV offering a lower unit cost for energy, while WT provides more consistent energy generation. This means that under the current base case assumption, it is economically reasonable to construct stand-alone RES production for hydrogen infrastructure without grid connections.

Besides the economics, the performance of each case studies is also analyzed using the two technical indicators, i.e., the electrolyzer utilization ratio and renewable curtailment ratio, which are also summarized in the bottom section of Table 2-3. It is found that grid connection can increase electrolyzer utilization and reduce renewable curtailment. The electrolyzer utilization of the grid-connected 2025 Base Case is 58.8%, which is higher than the other cases without grid connection. Cases without grid connection require a large electrolyzer (see Table 2-3) with a lower utilization rate due to variations in renewable energy availability. Similar observations are also made for the liquefaction units, where the utilization of the component decreases significantly in the PV-only and WT-only cases to 26.58% and

65.49%, respectively (see Table 2-3). Under these scenarios, a larger liquefaction unit is required to provide liquefied hydrogen during the limited availability of renewable energy, which is economically disadvantageous given that the liquefaction unit is an expensive piece of equipment. On the renewable curtailment, the grid-connected 2025 Base Case only curtails 7.9% of the renewables, compared to the 9.3%, 31.2% and 15.2% of RE-Only, PV-Only and WT-Only Cases, respectively. Under the current commercial availability of electrolyzers, further increasing electrolyzer capacity to utilize excess renewable energy is more expensive than curtailing the excess energy. This makes the system not only costly but also inefficient, highlighting the importance of reducing electrolyzer costs to enable a more efficient and renewable hydrogen production system.

2.4.2.2 Impacts by Technology Development

To study how potential technology development and market expansion can impact the optimal system sizing and cost, the 2050 Case is set up to compare the grid-connected cases using projected techno-economic values in 2050 (see Table 2-1). As shown in Table 2-3, the expected breakthroughs in technology and market penetration by 2050 reduce the total cost of the airport hydrogen system by 44.3%, along with increased capacities of several components. Due to decreased RES unit costs in 2050, the PV capacity increases significantly by 41.4%, while the WT capacity decreases by 22.3%. However, the cost breakdown in Table 2-3 shows that, despite the larger PV capacity in the 2050 Case, the total CAPEX is still 12.9% lower than in the 2025 Base Case due to reduced unit costs. Similar trends are observed in the hydrogen subsystem components. With projected improvements in electrolyzer efficiency and unit cost, the electrolyzer capacity in the 2050 Case increases by 51.4%, while the annualized electrolyzer cost drops by 54.4% due to the lower unit price (see Table 2-3).

It is also noted that the liquefaction unit remains the most expensive component in the entire system, despite the prospective reductions in both its unit cost and specific energy consumption. The capacity of the liquefaction unit remains unchanged from the 2025 Base Case to the 2050 Case, as it would be still quite expensive and inefficient to fit a larger unit into the system even in the 2050 Case.

Figure 2-9 shows that LCOH decreased to US$4.43/kg (or US$0.13/kWh) in the 2050 Case, down from US$7.45/kg in the 2025 Base Case. This value is lower and close to the higher end of recent jet fuel prices (i.e., US$1.72/kg, or US$0.14/kWh). This shows that with technological development, using hydrogen can deliver the same amounts of energy at similar costs to jet fuels.

The technical indicators of the two case studies are also analyzed. The EIS of the 2050 Case rises to almost unity (i.e., 0.99) from the value of 0.80 in the 2025 Base Case (as is seen in Table 2-3). This indicates that the reduction in cost and improvement in efficiency allows the system to be almost independent from the grid while maintaining its cost-effectiveness. It is also seen that the 2050 Case has lower renewable curtailment (i.e., 4.2%), which is lower than the 2025 Base Case at 7.9%. This is primarily due to the larger and cheaper electrolyzer with larger GH2 storage in the 2050 Case, which allows more renewable energy to be utilized for hydrogen production.

2.5 Conclusion

In this chapter, a MILP model has been constructed to study the optimal sizing of hydrogen infrastructure at Toronto Pearson Airport in Ontario, Canada, incorporating on-site production, storage, and refueling hydrogen-powered aircrafts. We also conducted sensitivity analyses on the impacts of component parameters such as the cost and efficiency and compared various system configurations and their economic performances under different case studies.

The optimal solution for the grid-connected 2025 Base Case reports an LCOH of US$7.45/kg of LH2, demonstrating a good degree of consistency with similar systems and scenarios reported in the literature. RES generation constitutes a dominant share of the energy supply to the hydrogen system. Sensitivity analyses reveal that the system's sizing composition and economics are highly sensitive to changes in the unit costs of electrolyzer, PV and WT. A large increase in the unit costs of these components can lead to a complete change in system configuration and operation strategy. Lowering electrolyzer costs could greatly enhance the cost-effectiveness of the hydrogen infrastructure, providing stronger economic incentives for adopting hydrogen as an aviation fuel.

Meanwhile, powering the hydrogen infrastructure using only one type of RES without grid connections results in very high LCOH. This is likely attributed to the limitations of individual RES technologies, such as the restricted daily availability of PV generation and the high costs associated with WT systems. Combining PV and WT in the RES-only configuration shows higher energy curtailment and lower energy utilization compared to the grid-connected 2025 Base Case, but similar LCOH’s.

With technological advancements, the 2050 Case indicates an increase in grid independence, rising to 0.99 from the value of 0.80 in the 2025 Base Case. This improvement is primarily driven by the projected cost reductions in RES and hydrogen technologies. The capital cost reductions lead to a larger RES and electrolyzer subsystems. Compared to the 2025 Base Case, the PV system capacity and

electrolyzer capacity increase by 41.4% and 51.4%, respectively, in the 2050 Case, while the overall system cost decreases by 44.2%. The LCOH decreases to US$4.43/kg LH2 in the 2050 Case, which equates to US$0.13/kWh, showing cost competitiveness with jet fuels.

Acknowledgement:

The contents in this chapter are in a manuscript that is under review:

Zhen Ye, Wenrui Ye, John Wen, Xiaoyu. Wu, “Planning renewable hydrogen infrastructure for airports,” Energy, under review, 2025

Chapter 3 Life Cycle Analysis of Airport Hydrogen System

3.1 Introduction

Hydrogen has long been regarded as a clean fuel; however, it is important to evaluate the degree of "cleanness" of hydrogen by considering the full life cycle of its production and use. This chapter presents a well-to-pump LCA developed for the airport hydrogen system described and studied in the previous chapter. It begins with a system description that defines the life cycle boundaries, followed by an inventory analysis of the hydrogen system components. The chapter concludes with the results and discussion of the CI assessment based on the inventory data. This chapter aims to address the following questions:

1. What is the life cycle CI of hydrogen production from the renewable-based airport hydrogen system?
2. What factors contribute to carbon emissions in the hydrogen life cycle?
3. How does the airport hydrogen system perform compared to the kerosene counterpart, regarding carbon emissions?

3.2 LCA System Description

The scope of the LCA in this study is illustrated in Figure 3-1, which highlight the system boundary of the airport hydrogen system proposed in Chapter 2 and describes the interactions between different upstream and downstream life cycle stages, including raw material extraction and processing, manufacturing of system components, and fuel production, all of which account for associated emissions. This LCA study aims to evaluate the well-to-pump environmental impact by considering the emissions associated with the raw materials and manufacturing of the seven major subsystem components, including the PV panels, WT, electrolyzer stacks, compressor, liquefaction unit, battery, GH2 and LH2 storage subsystems (as seen in Figure 3-1). The impact of aircraft production and operation is not included in the boundary of this study due to data paucity. The case studies that involve only the sustainable energy sources from Chapter 2 are studied for this LCA, with RE-Only case study as the baseline for comparison.

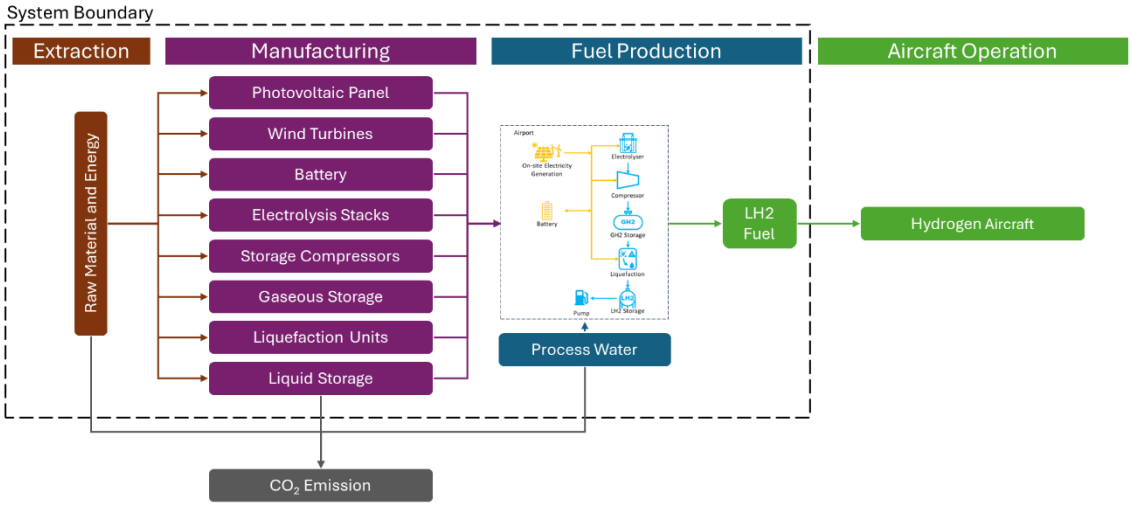


Figure 3-1. Schematic and system boundary of the well-to-pump life cycle assessment of the airport hydrogen system.

3.3 Life Cycle Inventory Analysis (LCIA)

ISO 14040 defines the LCI of a study as the data collection and calculation processes used to quantify the key inputs and outputs of a product system, including raw materials for manufacturing, energy consumption, waste, and emissions [66]. In this LCA study, each subsystem involved in the airport hydrogen system has its own detailed inventory, which is then integrated into the overall life cycle system described in Figure 3-1. For certain components such as the PV, WT, electrolyzer, and compressor, their LCIs are adopted from literature sources, which represent the materials required to manufacture a functional unit and can be scaled up linearly to the capacities determined in the selected case studies from Chapter 2. Other components, such as the liquefaction unit, GH2 storage, and LH2 storage, have LCIs determined using in-house assumptions along with literature descriptions of similar components. The following subsections present the final bill of materials (BOM) for the components whose LCIs are directly adopted from the literature. If a material appears in multiple manufacturing stages, the total weight of that material across all stages is summed and included in the final LCI. For the components with in-house derived LCIs, the assumptions and methods for their derivation will also be described in the following subsections.

3.3.1 PV Subsystem Inventory

Table 3-1. Summary of life cycle inventory of 1 kW PV functional unit (values adopted from [100], [101]**).**

Item	Unit	Quantity	Item	Unit	Quantity
Acetic acid	kg	0.20	Glass	kg	0.09
Acrylic acid	kg	0.03	Hydrochloric acid	kg	0.02
Acrylic binder	kg	0.01	Hydrogen fluoride	kg	0.03
Al Metallization paste	kg	0.28	Isopropanol	kg	0.89
Alkylbenzene sulfonate	kg	1.24	Lime	kg	0.14
Ammonia	kg	0.11	Natural gas	MJ	216.94
Argon	kg	2.88	Nitric acid	kg	0.19
Back Metallization paste	kg	0.01	Nitrogen	kg	5.75
Brass	kg	0.04	Phosphoryl chloride	kg	0.07
Ceramic	kg	0.48	Polyurethane	kg	2.32
Chromium steel	kg	0.01	PP	kg	0.21
CO_2	kg	0.84	Silane	kg	0.01
Concrete	kg	245.78	Silicon	kg	2.88
Copper	kg	3.15	Sodium hydroxide	kg	3.22
DGME	kg	1.55	Steel	kg	210.04
Electricity	kWh	205.14	Water	kg	15823.48
Front Metallization paste	kg	0.02	Zinc	kg	13.11

The data for the PV inventory in this study is collected from the ICA report on the LCI of photovoltaic systems, which provides a detailed BOM for different types of PV panels in various locations worldwide [100], as well as from the GREET model developed by Argonne National Laboratory [102].

For this study, the inventory for mono-Si PV panels manufactured in the U.S. is selected due to the high market share of the technology and its geographical relevance to the case study. The detailed LCI of the PV panel function unit can be found in Table A 1 of Appendix A. The PV panel used in this study is assumed to be a 1 kW functional unit, with an area of approximately 5 m², estimated based on commercially available products. Table 3-1 shows the total BOM from all stages involved in the manufacturing of a 1 kW mono-Si PV panel listed in Table A 1 of Appendix A, including the production of crystalline silicon, silicon wafers, the panel itself, and the balance of plant (BOP) per kW of PV panel.

3.3.2 WT Subsystem Inventory

Table 3-2. Summary of life cycle inventory of 1.65 MW WT functional unit (values adopted from [103]**).**

Item	Unit	Quantity
Aluminium	kg	66500
Cast Iron	kg	29300
Concrete	kg	805000
Copper	kg	57800
Electronics	kg	2500
Fiberglass	kg	27000
Oil	kg	39100
Plastic	kg	58200
Stainless Steel	kg	7800
Steel	kg	159900
Wood	kg	20700

The WT inventory for this study is adopted from Vestas' report on the manufacturing of V82 1.65 MW turbines [103]. In this LCA study, the 1.65 MW turbine is used as the functional unit for the WT

subsystem of the airport hydrogen system. The final CI contributed by the WT subsystem is calculated by linearly scaling the unit capacity to match the total WT capacity of the system. Table 3-2 presents the overall BOM in mass for manufacturing a single turbine unit, by adding up the material consumption for various components including the tower, nacelle, rotor, foundation for the turbine, as well as cables and transformer station for the BOP. The breakdown of these LCI materials of the WT subsystem components and BOP can be found in Table A 2 of Appendix A.

3.3.3 Electrolyzer Inventory

Table 3-3. Summary of life cycle inventory of 1 MW PEM electrolyzer functional unit (values adopted from [104]**).**

Item	Unit	Quantity	Item	Unit	Quantity
Aluminum	kg	268.94	Oil	kg	96.05
Au	kg	0.02	PET	kg	74.06
CeO_2	kg	0.03	Polyurethane	kg	0.26
Concrete	kg	5609.34	PP	kg	361.13
Copper	kg	351.96	Pt	kg	2.39
DI Water	kg	17.94	PTFE	kg	1.74
Elastomer	kg	117.93	SGL Carbon	kg	3.63
Electronics	kg	96.05	Stainless Steel	kg	4422.33
Ethelene glycol	kg	57.63	Steel	kg	7491.93
HDPE	kg	482.16	Sulfuric acid	kg	254.57
Hexanol	kg	0.05	Titanium	kg	219.77
Iridium	kg	2.72	Vulcan XC-72	kg	0.44
Isopropanol	kg	152.18	Zeolite	kg	96.05
Methanol	kg	168.65	Zinc	kg	0.29
Nafion	kg	19.62			

For the electrolyzer subsystem in this LCA study, the inventory for a 1 MW functional unit is developed from the work by Iyer et al. [104]. The BOM for the 1 MW unit is summarized in Table 3-3, presenting the total raw materials used in the production of various components of the electrolyzer stack as well as its BOP. Table A 3 of Appendix A shows the detailed BOM of electrolyzer stack and BOP production. In addition to the manufacturing of the electrolyzer stack, the system consumes 9 kg of water for every 1 kg of hydrogen produced [72]. The treatment of this water to a usable grade also results in emissions, which are included in the total emissions attributed to the electrolyzer subsystem.

3.3.4 Battery Storage Subsystem Inventory

The inventory for the BESS in this study is based on the GREET model. The GREET model provides the inventory for a commercial battery storage system of 2.4 MWh, which is used as the functional unit for the 10 MWh BESS in this study [101]. The battery cell technology in the BESS inventory is assumed to be Li-NMC, consistent with that used in Chapter 2. Table 3-4 summarizes the BOM by mass for the 2.4 MWh BESS, including the material weights for battery cell manufacturing and the BOP. The BOP of the BESS consists of the container, battery racks, and cables. The detailed battery inventory is provided in Table A 4.

Table 3-4. Summary of life cycle inventory of 2.4 MWh BESS functional unit (values adopted from GREET [101]**).**

Item	Unit	Quantity	Item	Unit	Quantity
Acrylic Binder	kg	119.89	Graphite	kg	2104.60
Active Material	kg	3742.67	LiPF6	kg	148.56
Aluminum	kg	1565.09	Plastic	kg	250.21
Copper	kg	1080.96	Polyurethane	kg	43.71
Dimethyl Carbonate	kg	413.10	Rubber	kg	2.61
Electronics	kg	71.67	Stainless steel	kg	413.10
Ethylene Carbonate	kg	413.10	Steel	kg	18613.03
Glycol	kg	497.81	Thermal Insulation	kg	43.00

3.3.5 Liquefaction Unit Inventory

The LCI for the liquefaction unit in this study is based on the work by Oeveren, who established the BOM for liquefaction plants with capacities ranging from 125 tpd to 500 tpd [105]. As reported in Chapter 2 of this work, the liquefaction unit capacities in the hydrogen airport system range from 9.51 tpd to 32.48 tpd across different case studies, which are scaled-down versions of the systems reported by Oeveren. In this study, the consumption of each material is extrapolated based on the daily liquefaction capacities from Oeveren's work to match the capacities reported in the case studies from Chapter 2. Table 3-5 presents the LCI for the 9.51 tpd liquefaction unit from the RE-Only case study in Chapter 2, along with data collected from literature [105].

Table 3-5. Life cycle inventory of hydrogen liquefaction system of various capacities.

	Unit	**This study**	**Literature Values** [105]		
Capacity	tpd	9.51	125	250	500
Concrete	kg	272937	4307402	7240516	14107621
Carbon Steel	kg	332031	499946	904418	2184640
Aluminum	kg	14259.3	157800	373150	757950
Copper	kg	27476.7	55473	102234	381645
Stainless Steel	kg	7742.09	120400	206500	400900

3.3.6 Storage Subsystem Inventory

The LCI of the storage subsystem in this study consists of the following components: a compressor for GH2 compression, GH2 cavern storage, and an LH2 storage tank. Table 3-6 summarizes the BOM required for the production of these components. The LCI of the compressor is collected as secondary data from Burkhardt et al., who reports a detailed LCI for a compressor with a 50-kW capacity [75], which is used as the functional unit in this study. The impacts contributed by the compressor in the system described in Chapter 2 are calculated by scaling the functional unit capacity linearly to the required system capacity.

The LCI of GH2 cavern storage is estimated as follows in this thesis. The basis for the cavern storage design is established using dimensions from Papadias and Ahluwalia [32], who described a lined rock cavern storage system measuring 62 m in diameter and 71 m in height, with a capacity of 500 t of GH2. The main materials used in lined rock cavern storage are stainless steel lining and concrete. The typical thickness of the lining is 15 mm [32], and the concrete layer is reported to have a thickness ranging from 0.8 m to 2 m [32], [106]. For better scalability, this study assumes that the storage structure is a perfect cylinder, with a constant aspect ratio based on the 62 m by 71 m design described in the literature, scaling linearly with storage capacity. This study also assumes a concrete thickness of 1 m, which aligns with the reported range from literature. Table 3-6 shows the sample BOM for the 500-t cavern storage, estimated using assumption made in this work and dimensions described by Papadias and Ahluwalia [32].

The material quantity required for the LH2 storage tank is estimated as follows. As mentioned in Chapter 2, to maintain cryogenic conditions, LH2 storage tanks are commonly designed as double-layered spherical structures. A detailed LH2 storage tank design is provided in a report by NASA, which suggests a 1.3 m gap between the inner and outer layers, both constructed with stainless steel [107]. While the wall thickness is not specified in the NASA report, it is specified by UL 142, which regulates the design of steel tanks for flammable liquid [108]. According to UL 142, large flammable liquid tanks with capacities between 50,000 and 76,000 gallons (capable of holding 13 to 20 tons of LH2) require a wall thickness of 9.27 mm [108]. This study assumes that the LH2 storage tank has a perfect spherical shape, with double stainless steel layers spaced 1.3 m apart, as described by NASA. For the tank wall thickness, the study adopts the 9.27 mm specification from the UL 142 standard, as the storage requirements in the case studies are close to this regulated range. Table 3-6 shows the sample BOM for a 70,000-gallon LH2 storage tank, calculated using the design described by NASA and the assumptions made in this report.

Table 3-6. Life cycle inventories of hydrogen storage system components, Top: Compressor (adopted from [75]); Mid: GH2 lined rock cavern storage; Bottom: LH2 storage tank.

Item	Unit	Quantity
Compressor		
Steel	kg	14012.5
Cast Iron	kg	739.8
Copper	kg	279.5
Aluminium	kg	77.3
PP	kg	64.7
Electronics	kg	26
GH2 Storage		
Concrete	kg	85066729
Stainless Steel	kg	4036499
LH2 Storage		
Stainless steel	kg	48538

3.4 Life Cycle Impact Analysis

For this LCA study, we developed an in-house LCA tool that integrates the LCIs of critical components from the airport hydrogen system described in the previous section with the system configurations reported in the case studies in Chapter 2. Using this tool, the total weight of each material from the LCIs for the PV, WT, and electrolyzer is obtained by linearly scaling up the functional unit to meet the required capacity, while the total weight of different materials involved in the manufacturing of the

liquefaction unit and the storage components are calculated by inputting the required capacity into the methods described in section 3.3.6.

For each of these materials, the in-house LCA tool computes their contribution to the life cycle impact of the on-site hydrogen production system in terms of CI, based on their respective carbon emission factors, expressed in kg CO_2-eq per kg of material used. The carbon emission factors and necessary assumptions for all materials appearing in the LCIs of this study can be found in Table A 4 of Appendix A. The life cycle carbon emissions of the hydrogen system are then calculated by summing the emissions associated with the manufacturing of each component, based on the materials used.

The tool also calculates the CI of the hydrogen produced in the system over its life cycle by dividing the total system life cycle emissions by the total hydrogen production over the 20 year system lifetime, where the total hydrogen production is calculated as the product of the annual hydrogen production reported from the simulation of the case study scenario using the MILP model from Chapter 2 and the system lifetime. Based on the required analysis, the tool can compute the life cycle CI of well to pump hydrogen production from the airport hydrogen system, expressed in terms of kg CO_2-eq per kg or per kWh of LH2 produced.

3.5 Results and Discussion

Figure 3-2 shows the life cycle CI of the three renewable-based case studies described in Chapter 2, with a breakdown of emission contributions from the manufacturing and operation of each component. The RE-Only case study, which serves as the baseline for this LCA, has a life cycle CI of 2.00 kg CO_2-eq/kg LH2. Among the three case studies, the PV-Only scenario has the highest CI at 4.07 kg CO_2-eq/kg LH2, while the WT-Only case has the lowest at 1.47 kg CO_2-eq/kg LH2. This makes the PV-Only scenario not only the most expensive (see Table 2-3), but also the most emission-intensive option. In all three case studies, it is evident from Figure 3-2 that the manufacturing of RES components accounts for the majority of the life cycle CI for H_2 production, contributing 92% (i.e., 59% from PV, 33% from WT), 94%, and 83% to the CI of the RE-Only, PV-Only, and WT-Only case studies, respectively. Besides the RES components, another major contributor to life cycle CI is the GH2 storage system, which accounts for 5% to 13% of the total CI across the various case studies.

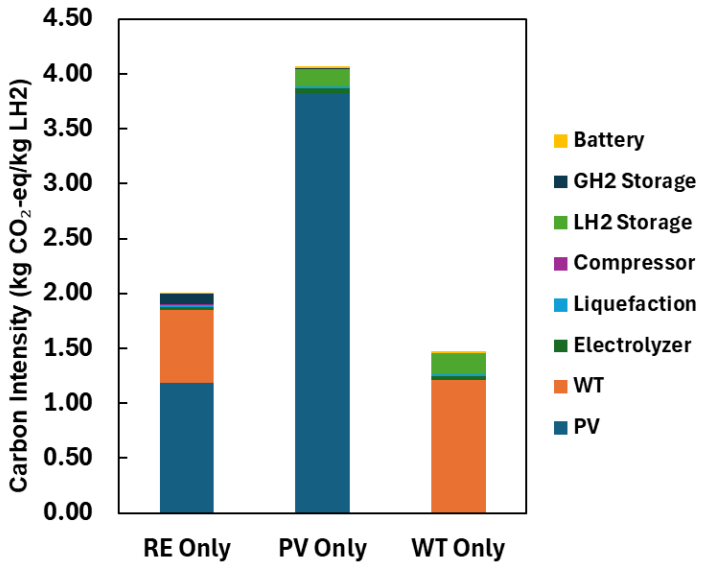


Figure 3-2. Component contributions to life cycle CI for RE-Only, PV-Only and WT-Only case studies.

To identify the root cause of the high emission intensity from certain system components, the top four most emission-intensive components are analyzed to examine the contribution of different raw materials in the manufacturing process. Figure 3-3 shows the CI contributions of various materials for the functional units of PV panels, WT, GH2 storage, and electrolyzer stacks. Note that materials contributing less than 0.5% of a component's manufacturing CI are grouped into the 'other materials' category for better visualization. It is revealed that steel and concrete are the two most CI-intensive materials in these components, with steel accounting for 47%, 37%, and 27% of the CI for the electrolyzer, PV, and WT, respectively, and concrete responsible for 73% of the CI from GH2 storage. Steel is heavily used in the manufacturing of the core component parts, as well as in the supporting structures within their BOPs and has a relatively high emission factor of 2.01 kg CO_2-eq/kg (see Table A 4) due to the carbon-intensive steel making process. On the other hand, for GH2 cavern storage, large amounts of concrete are required for the outer layer of the cavern, making up more than 90% of the total material weight. This contributes noticeably to life cycle emissions, particularly as storage requirements increase in the standalone RES technology case studies, despite the relatively low unit CI of concrete of 0.09 kg CO_2-eq/kg (see Table A 4). For the manufacturing of electrolyzer stacks, another major CI contributor is titanium, which is primarily used for the anode and bipolar plate of the stack, according to the GREET model [102]. Although titanium accounts for only 1.08% of the total LCI

weight (including BOP, see Table 3-3), its emission factor is extremely high (36.6 kg CO_2-eq/kg from Table A 4) due to the combustion processes involved in its production [102]. The production of a WT unit also results in significant carbon emissions from the use of aluminum and copper, mainly for the cables in the BOP (see Table A 2), as shown in Figure 3-3. Moreover, the crystalline silicon manufacturing stage for PV panel units consumes a large amount of cooling water (see Table A 1). Although the carbon emissions associated with processing cooling water are low per unit (see Table A 4), the high volume of consumption contributes significantly to the overall CI of PV panel production, accounting for 41% of the total.

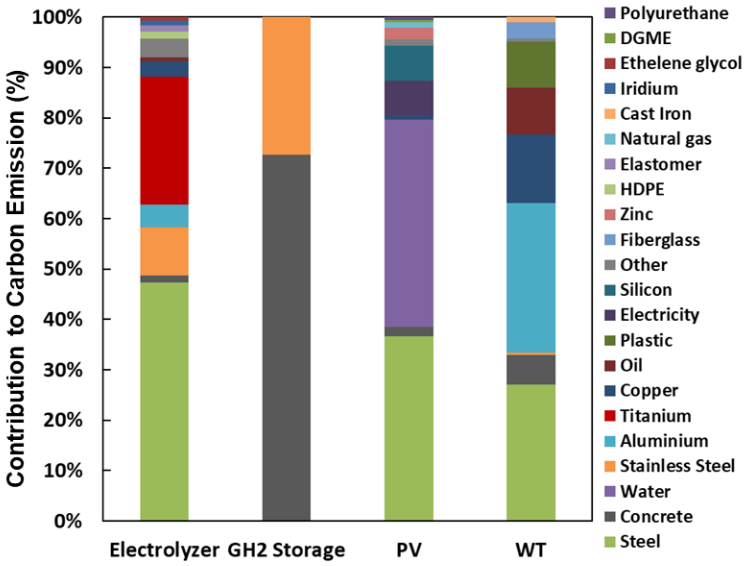


Figure 3-3. Material contributions to production CI for the functional unit of Electrolyzer, GH2 storage, PV and WT.

By examining the detailed breakdown of the CI contributions from materials in the LCI of the emission-intensive components in the hydrogen system, it becomes evident that a high CI contribution does not necessarily imply that certain technologies, particularly renewable technologies such as PV and WT, are not environmentally friendly or sustainable. Instead, the carbon emissions are primarily attributed to the use of fossil fuels in the production processes of certain materials, especially metal-based materials, which are required to build these technologies. This impact can be reduced over time as industries increasingly adopt sustainable energy sources in their processes, which would ultimately improve the carbon footprint of RES technology production and the hydrogen system as a whole.

The CI results are also compared to values from LCA studies on RES-powered PEM electrolysis hydrogen production in literature. While most literature focuses on GH2 as the end product, this study includes the liquefaction stage within the system boundary. As shown in Figure 3-2, the contributions of liquefaction and liquid storage to the overall CI are very low (0.69% and 0.03%, respectively). Therefore, the CI values from this study are still being compared to literature values for GH2 production. Table 3-7 summarizes the comparison between values from this study and literature values. In comparison, the CI results for the PV-Only and WT-Only scenarios align with findings from other researchers, with the CI value for the WT-Only case study falling closer to the lower end of the reported range. However, it is observed that the RE-Only scenario in this study reports a higher CI than similar scenarios in the literature. This variation is likely due to factors such as geographical location, system boundary definitions, the capacity mix between the renewable technologies and the scale of operations, all of which can influence the life cycle CI values reported in different studies.

The CI values from the case studies in this work are also compared to those of conventional jet fuel currently used in the aviation industry to assess the environmental benefits of switching to hydrogen-based aviation fuel. For consistency, the results are converted from a per-kilogram-of-H_2 basis to a per-kWh-of-H_2 basis: 0.06, 0.12, and 0.04 kg CO_2-eq/kWh H_2 for the RE-Only, PV-Only, and WT-Only case studies, respectively as shown in Table 3-7. The literature value for the CI of jet fuel is also shown in Table 3-7. At 0.32 kg CO_2-eq/kWh jet fuel, the CI of current aviation fuel is 3 to 8 times higher than that of on-site produced hydrogen fuel at airports in this study. These results demonstrate the environmental advantages of adopting hydrogen as an alternative aviation fuel, especially given the potential for further reductions in life cycle emissions through improvements in manufacturing processes and increased operational scale.

Table 3-7. Summary of life cycle CI comparison between this study and: Top, literature values per kg H_2; Bottom, jet fuel on a per kWh basis.

CI	Unit	Grid Mix	Product	Sources
2.00	kg CO_2-eq/kg H_2	PV+WT	LH2	This study
4.07	kg CO_2-eq/kg H_2	PV	LH2	This study
1.47	kg CO_2-eq/kg H_2	WT	LH2	This study
1.05-1.57	kg CO_2-eq/kg H_2	PV+WT	GH2	Garcia et al. [77]
4.07	kg CO_2-eq/kg H_2	PV	GH2	Vilbergsson et al. [109]
9.37	kg CO_2-eq/kg H_2	PV	GH2	Iyer et al. [73]
2.75	kg CO_2-eq/kg H_2	PV	GH2	Hermesmann and Müller [70]
1.58-2.95	kg CO_2-eq/kg H_2	PV	GH2	Al-Ghussain et al. [78]
3.1	kg CO_2-eq/kg H_2	PV	GH2	Al-Qahtani et al. [69]
1.99-7.1	kg CO_2-eq/kg H_2	PV	GH2	Garcia et al. [77]
0.35-1.9	kg CO_2-eq/kg H_2	WT	GH2	Al-Ghussain et al. [78]
0.86	kg CO_2-eq/kg H_2	WT	GH2	Al-Qahtani et al. [69]
0.85-2.2	kg CO_2-eq/kg H_2	WT	GH2	Garcia et al. [77]

CI	Unit	Grid Mix	Product	Sources
0.06	kg CO_2-eq/kWh H_2	PV+WT	LH2	This study
0.12	kg CO_2-eq/kWh H_2	PV	LH2	This study
0.04	kg CO_2-eq/kWh H_2	WT	LH2	This study
0.32	kg CO_2-eq/kWh jet fuel	-	Jet fuel	Jing et al. [110]

3.6 Conclusion

The well-to-pump LCA of the renewable energy-based case studies found that the life cycle CI ranges from 1.47 to 4.07 kg CO_2-eq/kg H_2, with the PV-Only case identified as the least favorable option for an on-site hydrogen production system at Toronto Pearson Airport in Ontario, Canada in terms of life cycle environmental impacts. The analysis indicates that RES components and cavern storage are among the major contributors to the life cycle CI of hydrogen fuel production. A closer examination of the LCI emissions of these top contributors suggests that the high CI is primarily due to fossil fuel

consumption during material processing, which is an impact that is expected to decline in the future with the increasing adoption of sustainable energy sources across industries. Furthermore, the life cycle CI of hydrogen production in the case study configurations shows a 3 to 8 times reduction compared to that of current jet fuel, highlighting the environmental benefits of adopting hydrogen as an aviation fuel.

Chapter 4 Conclusion and Future Work

4.1 Conclusion

The first project of the thesis, presented in Chapter 2, addresses the early adoption of hydrogen-based commercial aviation in Canada, using a MILP model developed to optimize the sizing of airport hydrogen infrastructure, including on-site production, storage, and refueling of hydrogen-powered aircraft. In the grid-connected 2025 Base Case, the LCOH is estimated to be US$7.45/kg LH2, similar to literature-reported values. The Base Case results also show that RES provide the majority of the system's energy. The use of GH2 cavern storage system allows for bulk storage and enables better RE utilization across different seasons. Sensitivity analyses highlight that system design and economics are highly influenced by the unit costs of the electrolyzer, GH2 storage, PV, and WT. Significant unit cost increases can lead to entirely different configurations and operation strategies, while unit cost reductions, especially in the electrolyzer, greatly improve system viability. Scenarios using a single RES technology without grid support lead to much higher LCOH due to the limitations of individual technologies, though combining PV and WT improves utilization and curtailment while achieving a similar LCOH to the Base Case. Looking ahead, the 2050 Case reflects technological advancements and cost reductions, leading to nearly full grid independence. These cost declines enable larger PV and electrolyzer, increasing by 41.4% and 51.4%, while reducing overall system cost by 44.2%. As a result, the LCOH drops to US$4.43/kg LH2, or US$0.13/kWh, showing competitiveness with jet fuels.

The second focus of this thesis is presented in Chapter 3, which examines the environmental impact of on-site hydrogen production at the airport. The well-to-pump LCA of the renewable energy-based case studies from Chapter 2 shows life cycle CI ranging from 1.47 to 4.07 kg CO_2-eq/kg LH2, with the PV-Only case having the highest impact and WT-Only being the most environmentally favorable. Major sources of carbon emissions include RES components and cavern storage, primarily due to fossil fuel use in material processing. This highlights the need for clean energy adoption across other industries in parallel with hydrogen-based aviation to achieve greater sustainability. Overall, the LH2 production in the case studies show a 3 to 8 times lower CI than current jet fuel, demonstrating strong environmental benefits of hydrogen-based aviation.

Case studies on the economics and carbon emissions reported in Chapter 2 and Chapter 3, respectively can provide additional insights when considered together. Between the two renewable technologies, PV panels appear to be the cheaper option in terms of unit cost per kW ($650/kW). However, powering

hydrogen production using a standalone PV configuration emerges as the least viable option in the case study of Toronto Pearson Airport in Ontario, Canada, due to its weak economic feasibility and poor life cycle emissions. This underperformance is primarily attributed to the inconsistent production patterns of PV, which necessitate significantly larger system capacities for all components. This, combined with its high life cycle emission contribution, ultimately leads to higher costs and life cycle emissions. The WT-Only configuration, on the other hand, is among the more expensive options in the case studies using 2025 techno-economic parameters, but it offers the lowest life cycle emissions. This indicates a potential trade-off between sustainability and economic feasibility, which should be considered when making decisions about the optimal early-stage on-site hydrogen production strategy at an airport.

4.2 Limitation and Future Work

The airport hydrogen system modeling analysis relies on data interpretation from multiple data sources, which may involve assumptions or approximations due to gaps in publicly available or high-resolution data. In particular, the parameters regarding the future techno-economic case are subjected to the limitations in the projection of technology costs and more importantly, technological development. Moreover, more technical details of liquefaction technology operation would benefit the modelling accuracy on the liquefying process. These assumptions might affect the accuracy of estimating the cost and technical availability of the technology involved in the airport hydrogen system.

This study assumes a fixed flight schedule to represent hydrogen demand, which simplifies the modeling but may not reflect realistic operational dynamics. Incorporating a more detailed and variable flight schedule would enable the development of a more realistic model and the optimization of the system's operational strategy. Additionally, the analysis relies on the most recent RES generation profile, without accounting for historical variability. Future work should include a more generic RES profile that incorporates uncertainties and fluctuations observed in historical data to improve the robustness of the results.

Furthermore, the current study adopts MILP to model the airport hydrogen system, where the constraints representing the energy flow and component operation are in linear relationships, which may not fully capture the complex interactions between subsystems. For example, the electrolyzer efficiency varies at different power load in an non-linear relation. These limitations can lead to inaccuracies in simulating system performance, especially under variable and uncertain operating environments. Future research could adopt a non-linear optimization framework to represent the energy

flows more accurately and support the development of a more dynamic and realistic system optimization model. Such an approach would allow for a more faithful representation of the physical and operational characteristics of each subsystem, enabling better decision-making in the design, sizing, and real-time operation of the integrated energy system.

For the LCA on the airport hydrogen system, the current study considers only CI as the evaluation metric for the life cycle impacts of the airport hydrogen system, which limits the scope of sustainability assessment. Future study can be conducted with a more comprehensive analysis including other commonly used indicators such as life cycle energy consumption, acidification, radiation, human toxicity, and land use. These factors are especially important given the involvement of PV, WT and the electrolyzer which, despite their low emissions during operation, have notable upstream impacts related to material extraction, manufacturing, and land requirements. Including these additional metrics would provide a more holistic understanding of the system's environmental performance and support more informed decision-making in future design and policy work.

The current LCA study adopts a Well-to-Pump system boundary, focusing solely on the life cycle impacts of hydrogen production from the airport hydrogen system. This approach excludes downstream processes such as aircraft operation and manufacturing, which are critical components of the full aviation value chain. To provide a more comprehensive assessment of hydrogen-based aviation, future work should expand the system boundary to include these additional stages. This would offer a clearer picture of the overall environmental impacts during early adoption and better inform comparisons with conventional aviation fuels.

Moreover, future work should incorporate optimization efforts that jointly consider both techno-economic performance and environmental impacts. Results from this study have shown that certain configurations, such as the WT-only case, perform well in terms of life cycle CI but rank among the more expensive options from a cost perspective. This highlights the trade-offs between sustainability and economic feasibility in system design. To address this, a multi-objective optimization framework could be developed to identify system configurations that offer a more balanced performance across both environmental and economic criteria. This would enable more informed decision-making by revealing the trade-offs and potential alignments between economic and environmental objectives, ultimately helping to identify system configurations that are both sustainable and cost-effective for hydrogen infrastructure development.

References

[1] IEA(2020), “World air passenger traffic evolution, 1980-2020,” Paris, Dec. 2020. Accessed: Jul. 07, 2025. [Online]. Available: https://www.iea.org/data-and-statistics/charts/world-air-passenger-traffic-evolution-1980-2020,

[2] Bureau of Transportation Statistics, “Bureau of Transportation Statistics F41 Schedule P12A ,” Aug. 2025.

[3] U.S. Energy Information Administration, “U.S. Year-to-Date Daily Average Supply and Disposition of Crude Oil and Petroleum Products (December 2019),” Dec. 2019. Accessed: Jul. 07, 2025. [Online]. Available: https://www.eia.gov/petroleum/supply/monthly/archive/2019/2019_12/pdf/table4.pdf

[4] IEA (2025), “CO2 emissions in aviation in the Net Zero Scenario, 2000-2030,” Paris, Jan. 2025. Accessed: Jul. 07, 2025. [Online]. Available: https://www.iea.org/data-and-statistics/charts/co2-emissions-in-aviation-in-the-net-zero-scenario-2000-2030

[5] IEA, “Energy related CO2 emissions, 1990-2019,” Feb. 2020. Accessed: Jul. 07, 2025. [Online]. Available: https://www.iea.org/data-and-statistics/charts/energy-related-co2-emissions-1990-2019

[6] Robert J. Blaszczak, “Nitrogen Oxides (NOx), Why and How They are Controlled,” Research Triangle Park,NC, Nov. 1999. Accessed: Jul. 07, 2025. [Online]. Available: https://www3.epa.gov/ttncatc1/cica/other7_e.html

[7] P. Su-ungkavatin, L. Tiruta-Barna, and L. Hamelin, “Biofuels, electrofuels, electric or hydrogen?: A review of current and emerging sustainable aviation systems,” *Prog Energy Combust Sci*, vol. 96, p. 101073, 2023, doi: https://doi.org/10.1016/j.pecs.2023.101073.

[8] M. Wang *et al.*, “Biomass-derived aviation fuels: Challenges and perspective,” *Prog Energy Combust Sci*, vol. 74, pp. 31–49, 2019, doi: https://doi.org/10.1016/j.pecs.2019.04.004.

[9] Nikita Pavlenko and Stephanie Searle, “Assessing the sustainability implications of alternative aviation fuels,” Mar. 2021. Accessed: Jul. 07, 2025. [Online]. Available: https://theicct.org/publication/assessing-the-sustainability-implications-of-alternative-aviation-fuels/

[10] E. S. Van der Sman, B. Peerlings, J. Kos, R. Lieshout, and T. Boonekamp, “Destination 2050,” Netherlands Aerospace Centre NLR, 2020. Accessed: Jan. 22, 2025. [Online]. Available: http://hdl.handle.net/10921/1555

[11] M. Braun, W. Grimme, and K. Oesingmann, “Pathway to net zero: Reviewing sustainable aviation fuels, environmental impacts and pricing,” *J Air Transp Manag*, vol. 117, p. 102580, 2024, doi: https://doi.org/10.1016/j.jairtraman.2024.102580.

[12] ROBERT THOMSON, MAXIM NAZUKIN, NIKHIL SACHDEVA, and NICOLAS MARTINEZ, “Aircraft Electrical Propulsion – The Next Chapter of Aviation?,” London, UK, 2017.

[13] NASA, “X-57 Maxwell Overview.” Accessed: Jul. 07, 2025. [Online]. Available: https://www.nasa.gov/centers-and-facilities/armstrong/x-57-maxwell/

[14] Eviation, “Fly the Future,” Eviation . Accessed: Jul. 07, 2025. [Online]. Available: https://www.eviation.com/

[15] J. Ribeiro *et al.*, “Environmental assessment of hybrid-electric propulsion in conceptual aircraft design,” *J Clean Prod*, vol. 247, p. 119477, 2020, doi: https://doi.org/10.1016/j.jclepro.2019.119477.

[16] Airbus, “E-Fan X,” AIRBUS. Accessed: Jul. 07, 2025. [Online]. Available: https://www.airbus.com/en/innovation/low-carbon-aviation/hybrid-and-electric-flight/e-fan-x

[17] B. Khandelwal, A. Karakurt, P. R. Sekaran, V. Sethi, and R. Singh, “Hydrogen powered aircraft : The future of air transport,” *Progress in Aerospace Sciences*, vol. 60, pp. 45–59, 2013, doi: https://doi.org/10.1016/j.paerosci.2012.12.002.

[18] M. Carmo, D. L. Fritz, J. Mergel, and D. Stolten, “A comprehensive review on PEM water electrolysis,” *Int J Hydrogen Energy*, vol. 38, no. 12, pp. 4901–4934, 2013, doi: https://doi.org/10.1016/j.ijhydene.2013.01.151.

[19] AIRBUS, “ZEROe.” Accessed: Dec. 28, 2024. [Online]. Available: https://www.airbus.com/en/innovation/energy-transition/hydrogen/zeroe

[20] ZeroAvia, “De Havilland Canada and ZeroAvia Announce Memorandum of Understanding (MOU) to Develop Hydrogen-Electric Engine Program for Dash 8-400 Aircraft.”

[21] Robert Thomson, “Hydrogen: A future fuel for aviation?,” Mar. 2020. Accessed: Dec. 28, 2024. [Online]. Available: https://www.rolandberger.com/en/Insights/Publications/Hydrogen-A-future-fuel-for-aviation.html

[22] P. Nikolaidis and A. Poullikkas, “A comparative overview of hydrogen production processes,” *Renewable and Sustainable Energy Reviews*, vol. 67, pp. 597–611, 2017, doi: https://doi.org/10.1016/j.rser.2016.09.044.

[23] M. Ji and J. Wang, “Review and comparison of various hydrogen production methods based on costs and life cycle impact assessment indicators,” *Int J Hydrogen Energy*, vol. 46, no. 78, pp. 38612–38635, 2021, doi: https://doi.org/10.1016/j.ijhydene.2021.09.142.

[24] J. Brito, F. Pinto, A. Ferreira, M. A. Soria, and L. M. Madeira, “Steam reforming of biomass gasification gas for hydrogen production: From thermodynamic analysis to experimental validation,” *Fuel Processing Technology*, vol. 250, p. 107859, 2023, doi: https://doi.org/10.1016/j.fuproc.2023.107859.

[25] Z. Navas-Anguita, D. García-Gusano, J. Dufour, and D. Iribarren, “Revisiting the role of steam methane reforming with CO2 capture and storage for long-term hydrogen production,” *Science of The Total Environment*, vol. 771, p. 145432, 2021, doi: https://doi.org/10.1016/j.scitotenv.2021.145432.

[26] S. Sebbahi *et al.*, “A comprehensive review of recent advances in alkaline water electrolysis for hydrogen production,” *Int J Hydrogen Energy*, vol. 82, pp. 583–599, 2024, doi: https://doi.org/10.1016/j.ijhydene.2024.07.428.

[27] S. Shiva Kumar and H. Lim, “An overview of water electrolysis technologies for green hydrogen production,” *Energy Reports*, vol. 8, pp. 13793–13813, 2022, doi: https://doi.org/10.1016/j.egyr.2022.10.127.

[28] K. T. Møller, T. R. Jensen, E. Akiba, and H. Li, “Hydrogen - A sustainable energy carrier,” *Progress in Natural Science: Materials International*, vol. 27, no. 1, pp. 34–40, 2017, doi: https://doi.org/10.1016/j.pnsc.2016.12.014.

[29] Bruce S *et al.*, “Opportunities for hydrogen in commercial aviation,” 2020. Accessed: Jul. 07, 2025. [Online]. Available: https://www.csiro.au/en/work-with-us/services/consultancy-strategic-advice-services/CSIRO-futures/Energy/hydrogen-commercial-aviation

[30] Hydrogen and Fuel Cell Technologies Office, “3.2 Hydrogen Delivery,” 2015.

[31] “The Future of Energy Storage.” Accessed: Mar. 27, 2025. [Online]. Available: https://energy.mit.edu/research/future-of-energy-storage/

[32] D. D. Papadias and R. K. Ahluwalia, “Bulk storage of hydrogen,” *Int J Hydrogen Energy*, vol. 46, no. 70, pp. 34527–34541, 2021, doi: https://doi.org/10.1016/j.ijhydene.2021.08.028.

[33] R. I. A. Rathnayaka and P. G. Ranjith, “Hydrogen storage in unlined rock caverns: An insight on opportunities and challenges,” *Int J Hydrogen Energy*, vol. 72, pp. 1023–1037, 2024, doi: https://doi.org/10.1016/j.ijhydene.2024.05.447.

[34] NREL, “Costs of Storing and Transporting Hydrogen,” 1998.

[35] J. Hoelzen, L. Koenemann, L. Kistner, F. Schenke, A. Bensmann, and R. Hanke-Rauschenbach, “H2-powered aviation – Design and economics of green LH2 supply for airports,” *Energy Conversion and Management: X*, vol. 20, p. 100442, 2023, doi: https://doi.org/10.1016/j.ecmx.2023.100442.

[36] M. Genovese and P. Fragiacomo, “Hydrogen refueling station: Overview of the technological status and research enhancement,” *J Energy Storage*, vol. 61, p. 106758, 2023, doi: https://doi.org/10.1016/j.est.2023.106758.

[37] D. Apostolou and G. Xydis, “A literature review on hydrogen refuelling stations and infrastructure. Current status and future prospects,” *Renewable and Sustainable Energy Reviews*, vol. 113, p. 109292, 2019, doi: https://doi.org/10.1016/j.rser.2019.109292.

[38] G. D. Brewer, “Hydrogen usage in air transportation,” *Int J Hydrogen Energy*, vol. 3, no. 2, pp. 217–229, 1978, doi: https://doi.org/10.1016/0360-3199(78)90020-4.

[39] P. F. Korycinski, “Air terminals and liquid hydrogen commercial air transports,” *Int J Hydrogen Energy*, vol. 3, no. 2, pp. 231–250, 1978, doi: https://doi.org/10.1016/0360-3199(78)90021-6.

[40] G. D. Brewer, “LH2 airport requirements study,” Oct. 1976.

[41] L. Jones, C. Wuschke, and T. Z. Fahidy, “Model of a cryogenic liquid-hydrogen pipeline for an airport ground distribution system,” *Int J Hydrogen Energy*, vol. 8, no. 8, pp. 623–630, 1983, doi: https://doi.org/10.1016/0360-3199(83)90231-8.

[42] M. J. Sefain, “Hydrogen aircraft concepts and ground support,” Cranfield University, 2005.

[43] M. Janić, “Greening commercial air transportation by using liquid hydrogen (LH2) as a fuel,” *Int J Hydrogen Energy*, vol. 39, no. 29, pp. 16426–16441, 2014, doi: https://doi.org/10.1016/j.ijhydene.2014.08.011.

[44] F. Haglind, A. Hasselrot, and R. Singh, “Potential of reducing the environmental impact of aviation by usinghydrogen Part III: Optimum cruising altitude and airportimplications,” *The Aeronautical Journal (1968)*, vol. 110, no. 1110, pp. 553–565, 2006, doi: DOI: 10.1017/S0001924000013853.

[45] R. Fusaro, V. Vercella, D. Ferretto, N. Viola, and J. Steelant, “Economic and environmental sustainability of liquid hydrogen fuel for hypersonic transportation systems,” *CEAS Space Journal*, vol. 12, no. 3, pp. 441–462, 2020, doi: 10.1007/s12567-020-00311-x.

[46] J. Mangold *et al.*, “Refueling of LH2 Aircraft—Assessment of Turnaround Procedures and Aircraft Design Implication,” *Energies (Basel)*, vol. 15, no. 7, 2022, doi: 10.3390/en15072475.

[47] J. Hoelzen, M. Flohr, D. Silberhorn, J. Mangold, A. Bensmann, and R. Hanke-Rauschenbach, “H2-powered aviation at airports – Design and economics of LH2 refueling systems,” *Energy Conversion and Management: X*, vol. 14, p. 100206, 2022, doi: https://doi.org/10.1016/j.ecmx.2022.100206.

[48] D. Mahajan, K. Tan, T. Venkatesh, P. Kileti, and C. R. Clayton, “Hydrogen Blending in Gas Pipeline Networks—A Review,” *Energies (Basel)*, vol. 15, no. 10, 2022, doi: 10.3390/en15103582.

[49] S.-K. Seo, D.-Y. Yun, and C.-J. Lee, “Design and optimization of a hydrogen supply chain using a centralized storage model,” *Appl Energy*, vol. 262, p. 114452, 2020, doi: https://doi.org/10.1016/j.apenergy.2019.114452.

[50] M.-K. Kazi, F. Eljack, M. M. El-Halwagi, and M. Haouari, “Green hydrogen for industrial sector decarbonization: Costs and impacts on hydrogen economy in qatar,” *Comput Chem Eng*, vol. 145, p. 107144, 2021, doi: https://doi.org/10.1016/j.compchemeng.2020.107144.

[51] A. X. Y. Mah *et al.*, “Spatial optimization of photovoltaic-based hydrogen-electricity supply chain through an integrated geographical information system and mathematical modeling

approach," *Clean Technol Environ Policy*, vol. 24, no. 1, pp. 393–412, 2022, doi: 10.1007/s10098-021-02235-4.

[52] G. Yang, Y. Jiang, and S. You, "Planning and operation of a hydrogen supply chain network based on the off-grid wind-hydrogen coupling system," *Int J Hydrogen Energy*, vol. 45, no. 41, pp. 20721–20739, 2020, doi: https://doi.org/10.1016/j.ijhydene.2020.05.207.

[53] M. E. Demir and I. Dincer, "Cost assessment and evaluation of various hydrogen delivery scenarios," *Int J Hydrogen Energy*, vol. 43, no. 22, pp. 10420–10430, 2018, doi: https://doi.org/10.1016/j.ijhydene.2017.08.002.

[54] O. J. Guerra, J. Eichman, J. Kurtz, and B.-M. Hodge, "Cost Competitiveness of Electrolytic Hydrogen," *Joule*, vol. 3, no. 10, pp. 2425–2443, 2019, doi: https://doi.org/10.1016/j.joule.2019.07.006.

[55] J. Ochoa Robles, M. Giraud Billoud, C. Azzaro-Pantel, and A. A. Aguilar-Lasserre, "Optimal Design of a Sustainable Hydrogen Supply Chain Network: Application in an Airport Ecosystem," *ACS Sustain Chem Eng*, vol. 7, no. 21, pp. 17587–17597, Nov. 2019, doi: 10.1021/acssuschemeng.9b02620.

[56] Anna Nadia Cybulsky, "Techno-Economic Modeling and Optimization of Hydrogen Supply Chain for Aviation Demand," MASSACHUSETTS INSTITUTE OF TECHNOLOGY, Cambridge, MA, 2023.

[57] S. Alexandrou and D. Khatiwada, "Strategies for decarbonizing the aviation sector: Evaluating economic competitiveness of green hydrogen value chains - A case study in France," *Energy*, vol. 314, p. 134111, 2025, doi: https://doi.org/10.1016/j.energy.2024.134111.

[58] F. Schenke, J. Hoelzen, D. Bredemeier, L. Schomburg, A. Bensmann, and R. Hanke-Rauschenbach, "LH2 supply for the initial development phase of H2-powered aviation," *Energy Conversion and Management: X*, vol. 24, p. 100797, 2024, doi: https://doi.org/10.1016/j.ecmx.2024.100797.

[59] S. Rezaei, K. Alsamri, E. Simeoni, J. Huynh, and J. Brouwer, "Techno-economic and environmental analysis of clean hydrogen deployment: A case study of Los Angeles International Airport," *Energy Convers Manag*, vol. 340, p. 119946, 2025, doi: https://doi.org/10.1016/j.enconman.2025.119946.

[60] M. A. Giovanniello and X.-Y. Wu, “Hybrid lithium-ion battery and hydrogen energy storage systems for a wind-supplied microgrid,” *Appl Energy*, vol. 345, p. 121311, 2023, doi: https://doi.org/10.1016/j.apenergy.2023.121311.

[61] P. Marocco, D. Ferrero, E. Martelli, M. Santarelli, and A. Lanzini, “An MILP approach for the optimal design of renewable battery-hydrogen energy systems for off-grid insular communities,” *Energy Convers Manag*, vol. 245, p. 114564, 2021, doi: https://doi.org/10.1016/j.enconman.2021.114564.

[62] A. S. Jacob, R. Banerjee, and P. C. Ghosh, “Sizing of hybrid energy storage system for a PV based microgrid through design space approach,” *Appl Energy*, vol. 212, pp. 640–653, 2018, doi: https://doi.org/10.1016/j.apenergy.2017.12.040.

[63] D. Ding and X.-Y. Wu, “Optimization of Fuel Cell Electric Vehicle-to-Grid in Alberta by Mixed Integer Linear Programming,” in *2023 IEEE 11th International Conference on Smart Energy Grid Engineering (SEGE)*, 2023, pp. 43–47. doi: 10.1109/SEGE59172.2023.10274585.

[64] N. Kopacak, H. Cihan Güldorum, and O. Erdinc, “Implementation of a Decision-Making Approach for a Hydrogen-Based Multi-Energy System Considering EVs and FCEVs Availability,” *IEEE Access*, vol. 12, pp. 114705–114721, 2024, doi: 10.1109/ACCESS.2024.3441328.

[65] R. Caponi, E. Bocci, and L. Del Zotto, “On-site hydrogen refuelling station techno-economic model for a fleet of fuel cell buses,” *Int J Hydrogen Energy*, vol. 71, pp. 691–700, 2024, doi: https://doi.org/10.1016/j.ijhydene.2024.05.216.

[66] ISO, “ISO 14044:2006: Environmental management — Life cycle assessment — Requirements and guidelines ,” Geneva, CH, 2006.

[67] E. Cetinkaya, I. Dincer, and G. F. Naterer, “Life cycle assessment of various hydrogen production methods,” *Int J Hydrogen Energy*, vol. 37, no. 3, pp. 2071–2080, 2012, doi: https://doi.org/10.1016/j.ijhydene.2011.10.064.

[68] J. Dufour, D. P. Serrano, J. L. Gálvez, A. González, E. Soria, and J. L. G. Fierro, “Life cycle assessment of alternatives for hydrogen production from renewable and fossil sources,” *Int J*

Hydrogen Energy, vol. 37, no. 2, pp. 1173–1183, 2012, doi: https://doi.org/10.1016/j.ijhydene.2011.09.135.

[69] A. Al-Qahtani, B. Parkinson, K. Hellgardt, N. Shah, and G. Guillen-Gosalbez, "Uncovering the true cost of hydrogen production routes using life cycle monetisation," *Appl Energy*, vol. 281, p. 115958, 2021, doi: https://doi.org/10.1016/j.apenergy.2020.115958.

[70] M. Hermesmann and T. E. Müller, "Green, Turquoise, Blue, or Grey? Environmentally friendly Hydrogen Production in Transforming Energy Systems," *Prog Energy Combust Sci*, vol. 90, p. 100996, 2022, doi: https://doi.org/10.1016/j.pecs.2022.100996.

[71] K. Bareiß, C. de la Rua, M. Möckl, and T. Hamacher, "Life cycle assessment of hydrogen from proton exchange membrane water electrolysis in future energy systems," *Appl Energy*, vol. 237, pp. 862–872, 2019, doi: https://doi.org/10.1016/j.apenergy.2019.01.001.

[72] N. Gerloff, "Comparative Life-Cycle-Assessment analysis of three major water electrolysis technologies while applying various energy scenarios for a greener hydrogen production," *J Energy Storage*, vol. 43, p. 102759, 2021, doi: https://doi.org/10.1016/j.est.2021.102759.

[73] R. K. Iyer, J. H. Prosser, J. C. Kelly, B. D. James, and A. Elgowainy, "Life-cycle analysis of hydrogen production from water electrolyzers," *Int J Hydrogen Energy*, vol. 81, pp. 1467–1478, 2024, doi: https://doi.org/10.1016/j.ijhydene.2024.06.355.

[74] S. Ghandehariun and A. Kumar, "Life cycle assessment of wind-based hydrogen production in Western Canada," *Int J Hydrogen Energy*, vol. 41, no. 22, pp. 9696–9704, 2016, doi: https://doi.org/10.1016/j.ijhydene.2016.04.077.

[75] J. Burkhardt, A. Patyk, P. Tanguy, and C. Retzke, "Hydrogen mobility from wind energy – A life cycle assessment focusing on the fuel supply," *Appl Energy*, vol. 181, pp. 54–64, 2016, doi: https://doi.org/10.1016/j.apenergy.2016.07.104.

[76] J. Zhang, B. Ling, Y. He, Y. Zhu, and Z. Wang, "Life cycle assessment of three types of hydrogen production methods using solar energy," *Int J Hydrogen Energy*, vol. 47, no. 30, pp. 14158–14168, 2022, doi: https://doi.org/10.1016/j.ijhydene.2022.02.150.

[77] M. Garcia G. and S. Oliva H., "Technical, economic, and CO2 emissions assessment of green hydrogen production from solar/wind energy: The case of Chile," *Energy*, vol. 278, p. 127981, 2023, doi: https://doi.org/10.1016/j.energy.2023.127981.

[78] L. Al-Ghussain, M. Alrbai, S. Al-Dahidi, and Z. Lu, “Integrated assessment of green hydrogen production in California: Life cycle Greenhouse gas Emissions, Techno-Economic Feasibility, and resource variability,” *Energy Convers Manag*, vol. 311, p. 118514, 2024, doi: https://doi.org/10.1016/j.enconman.2024.118514.

[79] S. R. Pereira, T. Fontes, and M. C. Coelho, “Can hydrogen or natural gas be alternatives for aviation? – A life cycle assessment,” *Int J Hydrogen Energy*, vol. 39, no. 25, pp. 13266–13275, 2014, doi: https://doi.org/10.1016/j.ijhydene.2014.06.146.

[80] O. Siddiqui and I. Dincer, “A comparative life cycle assessment of clean aviation fuels,” *Energy*, vol. 234, p. 121126, 2021, doi: https://doi.org/10.1016/j.energy.2021.121126.

[81] S. Pfenninger and I. Staffell, “Long-term patterns of European PV output using 30 years of validated hourly reanalysis and satellite data,” *Energy*, vol. 114, pp. 1251–1265, 2016, doi: https://doi.org/10.1016/j.energy.2016.08.060.

[82] I. Staffell and S. Pfenninger, “Using bias-corrected reanalysis to simulate current and future wind power output,” *Energy*, vol. 114, pp. 1224–1239, 2016, doi: https://doi.org/10.1016/j.energy.2016.08.068.

[83] M. M. Rienecker *et al.*, “MERRA: NASA’s Modern-Era Retrospective Analysis for Research and Applications,” *J Clim*, vol. 24, no. 14, pp. 3624–3648, Jul. 2011, doi: 10.1175/JCLI-D-11-00015.1.

[84] A. Pena-Bello, E. Barbour, M. C. Gonzalez, M. K. Patel, and D. Parra, “Optimized PV-coupled battery systems for combining applications: Impact of battery technology and geography,” *Renewable and Sustainable Energy Reviews*, vol. 112, pp. 978–990, 2019, doi: https://doi.org/10.1016/j.rser.2019.06.003.

[85] M. Carmo, D. L. Fritz, J. Mergel, and D. Stolten, “A comprehensive review on PEM water electrolysis,” *Int J Hydrogen Energy*, vol. 38, no. 12, pp. 4901–4934, 2013, doi: https://doi.org/10.1016/j.ijhydene.2013.01.151.

[86] M. Aasadnia and M. Mehrpooya, “Large-scale liquid hydrogen production methods and approaches: A review,” *Appl Energy*, vol. 212, pp. 57–83, 2018, doi: https://doi.org/10.1016/j.apenergy.2017.12.033.

[87] S. Z. S. Al Ghafri *et al.*, “Hydrogen liquefaction: a review of the fundamental physics, engineering practice and future opportunities,” *Energy Environ. Sci.*, vol. 15, no. 7, pp. 2690–2731, 2022, doi: 10.1039/D2EE00099G.

[88] “Flightradar24.” Accessed: Mar. 27, 2025. [Online]. Available: https://www.flightradar24.com/

[89] FCHEA, “Road Map to a US Hydrogen Economy,” 2021.

[90] IEA, “IEA G20 Hydrogen report: Assumptions,” Dec. 2020.

[91] IRENA, “Green Hydrogen Cost Reduction: Scaling up Electrolysers to Meet the 1.5^0C Climate Goal,” Abu Dhabi, 2020.

[92] Hydrogen Council, “Hydrogen Insights 2021: A Perspective on Hydrogen Investment, Deployment and Cost Competitiveness.,” Jan. 2021.

[93] T. Zhang, J. Uratani, Y. Huang, L. Xu, S. Griffiths, and Y. Ding, “Hydrogen liquefaction and storage: Recent progress and perspectives,” *Renewable and Sustainable Energy Reviews*, vol. 176, p. 113204, 2023, doi: https://doi.org/10.1016/j.rser.2023.113204.

[94] L. Sens, Y. Piguel, U. Neuling, S. Timmerberg, K. Wilbrand, and M. Kaltschmitt, “Cost minimized hydrogen from solar and wind – Production and supply in the European catchment area,” *Energy Convers Manag*, vol. 265, p. 115742, 2022, doi: https://doi.org/10.1016/j.enconman.2022.115742.

[95] W. Cole, A. W. Frazier, and Augustine. Chad, “Cost Projections for Utility-Scale Battery Storage: 2021 Update,” Golden, CO, Jun. 2021.

[96] A. Ochoa Bique and E. Zondervan, “An outlook towards hydrogen supply chain networks in 2050 — Design of novel fuel infrastructures in Germany,” *Chemical Engineering Research and Design*, vol. 134, pp. 90–103, 2018, doi: https://doi.org/10.1016/j.cherd.2018.03.037.

[97] W. Ye *et al.*, “Component capacity optimization of a renewable energy system using data-driven two-stage algorithmic approach,” *Energy Convers Manag*, vol. 312, p. 118588, 2024, doi: https://doi.org/10.1016/j.enconman.2024.118588.

[98] M. P. A. E. C. H. Elizabeth Connelly, “Current Status of Hydrogen Liquefaction Costs,” Aug. 2019.

[99] U.S. Energy Information Administration, “U.S. Gulf Coast Kerosene-type jet fuel spot price fob (dollars per gallon).” Accessed: Mar. 27, 2025. [Online]. Available: https://www.eia.gov/dnav/pet/hist/eer_epjk_pf4_rgc_dpgD.htm

[100] Rolf Frischknecht, Philippe Stolz, Luana Krebs, Mariska de Wild-Scholten, and Parikhit Sinha, “Life Cycle Inventories and Life Cycle Assessments of Photovoltaic Systems 2020,” Dec. 2020.

[101] United States Department of Energy, “R&D GREET Life Cycle Assessment Model.” Accessed: Apr. 21, 2025. [Online]. Available: https://www.energy.gov/eere/rd-greet-life-cycle-assessment-model

[102] M. Wang *et al.*, “Greenhouse gases, Regulated Emissions, and Energy use in Technologies Model ® (2024 Excel),” Dec. 2024. doi: 10.11578/GREET-Excel-2024/dc.20241203.1.

[103] Vestas Wind Systems A/S, “Life cycle assessment of electricity produced from onshore sited wind power plants based on Vestas V82-1.65 MW turbines ,” Dec. 2006.

[104] R. Iyer, J. Kelly, and A. Elgowainy, “Electrolyzers for Hydrogen Production: Solid Oxide, Alkaline, and Proton Exchange Membrane,” Argonne, IL (United States), Oct. 2022. doi: 10.2172/1894304.

[105] T.A. van Oeveren, “Hydrogen Liquefaction: Life Cycle Analysis,” TU Delft, 2024.

[106] M. Masoudi, A. Hassanpouryouzband, H. Hellevang, and R. S. Haszeldine, “Lined rock caverns: A hydrogen storage solution,” *J Energy Storage*, vol. 84, p. 110927, 2024, doi: https://doi.org/10.1016/j.est.2024.110927.

[107] J. Fesmire, A. Swanger, J. Jacobson, and W. Notardonato, “Energy efficient large-scale storage of liquid hydrogen,” *IOP Conf Ser Mater Sci Eng*, vol. 1240, no. 1, p. 012088, May 2022, doi: 10.1088/1757-899X/1240/1/012088.

[108] Underwriters Laboratories Inc., “UL 142 Standard for Safety for Steel Aboveground Tanks for Flammable and Combustible Liquids,” Northbrook, IL, Dec. 2006.

[109] K. V Vilbergsson, K. Dillman, N. Emami, E. J. Ásbjörnsson, J. Heinonen, and D. C. Finger, “Can remote green hydrogen production play a key role in decarbonizing Europe in the future? A cradle-to-gate LCA of hydrogen production in Austria, Belgium, and Iceland,” *Int J*

Hydrogen Energy, vol. 48, no. 46, pp. 17711–17728, 2023, doi: https://doi.org/10.1016/j.ijhydene.2023.01.081.

[110] L. Jing *et al.*, "Understanding variability in petroleum jet fuel life cycle greenhouse gas emissions to inform aviation decarbonization," *Nat Commun*, vol. 13, no. 1, p. 7853, 2022, doi: 10.1038/s41467-022-35392-1.

[111] D. P. Fogliatti, S. A. Kemppainen, T. N. Kalnes, J. Fan, and D. R. Shonnard, "Life Cycle Carbon Footprint of Linear Alkylbenzenesulfonate from Coconut Oil, Palm Kernel Oil, and Petroleum-Based Paraffins," *ACS Sustain Chem Eng*, vol. 2, no. 7, pp. 1828–1834, Jul. 2014, doi: 10.1021/sc5001622.

[112] City of Winnipeg, "682-2012 Appendix 7: CO2 emission factors database," Winnipeg, 2012.

[113] Canada Energy Regulator / Régie de l'énergie du Canada, "Provincial and Territorial Energy Profiles – Canada," Canada Energy Regulator / Régie de l'énergie du Canada.

Appendix A. Detailed Life Cycle Inventories and Material Emission Factors

Table A 1 Detailed life cycle inventory of material requirements of different stages of PV panel production and BOP.

Item	Unit	Weight
PV Panel	**m2**	**1**
Wafer	m2	1.03
Front Metallization paste	kg	0.0034
Back Metallization paste	kg	0.0011
Al Metallization paste	kg	0.06
Ammonia	kg	0.02
Phosphoryl chloride	kg	0.01
Isopropanol	kg	0.18
Hydrochloric acid	kg	0.00
Hydrogen flouride	kg	0.00
Sodium hydroxide	kg	0.60
Lime	kg	0.02
Nitrogen	kg	1.15
Silane	kg	0.00
Water	kg	171.00
Electricity	kWh	17.70
CO_2	kg	0.17
Wafer	**m2**	**1**
CZ Silicon	kg	0.56
Glass	kg	0.01
Sodium hydroxide	kg	0.02
Hydrochloric acid	kg	0.00
Acetic acid	kg	0.04
Dipropylene glycol monomethyl ether	kg	0.30
Alkylbenzene sulfonate	kg	0.24
Acrylic acid	kg	0.00
Brass	kg	0.01

Chromium steel	kg	0.00
Steel	kg	0.01
Electricity	kWh	4.76
Natural gas	MJ	4.00
Water	kg	55.60
CZ Silicon	**kg**	**1.00**
Silicon	kg	1.00
Argon	kg	1.00
Hydrogen flouride	kg	0.01
Nitric acid	kg	0.07
Sodium hydroxide	kg	0.04
Ceramic	kg	0.17
Lime	kg	0.02
Electricity	kWh	32.00
Natural gas	MJ	68.20
Water	kg	5100.00
BOP	m2	1.00
PP	kg	0.04
Steel	kg	42.00
Zinc	kg	2.62
Concrete	kg	49.16
Polyurethane	kg	0.46
Glass	kg	0.01
Acrylic acid	kg	0.01
Copper	kg	0.63

Inventory of the manufacturing of the PV panel, wafer, and CZ silicon are adopted from the IEA report [100].

The BOP data is adopted from GREET [101].

Table A 2. Detailed life cycle inventory of material requirements of different parts of WT production and BOP.

Item	Unit	Weight
Tower		
Steel	kg	16100
Aluminum	kg	2600
Electronics	kg	2200
Plastic	kg	2000
Copper	kg	1300
Oil	kg	1000
Nacelle		
Cast Iron	kg	18000
Steel	kg	19300
Stainless steel	kg	7800
Fiberglass	kg	1800
Copper	kg	1600
Plastic	kg	1000
Aluminum	kg	500
Electronics	kg	300
Oil	kg	300
Rotor		
Cast Iron	kg	11300
Steel	kg	5700
Fiberglass	kg	25200
Foundation		
Concrete	kg	805000
Steel	kg	27000

Cables		
Aluminum	kg	63400
Plastic	kg	55200
Copper	kg	30900
Transformer		
Steel	kg	91800
Copper	kg	24000
Oil	kg	37800
Wood	kg	20700

Values of this table are adopted from Vestas' report [103].

Table A 3. Detailed life cycle inventory of material requirements of different parts and BOP of PEM electrolyzer stack.

Item	Unit	Weight
Main Stack		
SGL Carbon	kg	3.63
PTFE	kg	0.57
Methanol	kg	2.39
DI Water	kg	2.39
Vulcan XC-72	kg	0.44
Titanium	kg	56.72
Polyurethane	kg	0.26
Zinc	kg	0.29
Pt	kg	0.23
PTFE	kg	0.89
Nafion	kg	16.10
DI Water	kg	1.45
Hexanol	kg	0.05
Isopropanol	kg	152.18
Methanol	kg	152.15
Iridium	kg	2.72
Methanol	kg	14.11
DI Water	kg	14.11
Nafion	kg	3.52
CeO2	kg	0.03
Pt	kg	2.13
Titanium	kg	163.05
PP	kg	45.58
Sulfuric acid	kg	254.57
Au	kg	0.02
Pt	kg	0.02
PET	kg	11.73

Elastomer	kg	2.66
HDPE	kg	17.01
HDPE	kg	3.79
PET	kg	62.33
Elastomer	kg	0.01
Stainless Steel	kg	85.95
HDPE	kg	0.06
Copper	kg	6.18
HDPE	kg	0.26
PP	kg	8.19
Stainless Steel	kg	0.17
Stainless Steel	kg	0.23
Stainless Steel	kg	13.72
PTFE	kg	0.28
BOP		
Steel	kg	7491.93
Concrete	kg	5609.34
Stainless Steel	kg	4322.27
PP	kg	307.36
HDPE	kg	461.04
Copper	kg	345.78
Aluminum	kg	268.94
Elastomer	kg	115.26
Oil	kg	96.05
Zeolite	kg	96.05
Electronics	kg	96.05
Ethelene glycol	kg	57.63

Values of this table are collected from Iyer et al. [104]

Table A 4. Detailed life cycle inventory of material requirements of battery cell and BOP of battery energy system.

Item	Unit	Weight
Main Stack		
Active Material	kg	3742.67
Graphite	kg	2104.60
Acrylic acid	kg	119.89
Copper	kg	1025.59
Aluminium	kg	1565.09
$LiPF_6$	kg	148.56
Ethylene Carbonate	kg	413.10
Dimethyl Carbonate	kg	413.10
Plastic	kg	250.21
Steel	kg	1846.58
Stainless steel	kg	413.10
Rubber	kg	2.61
Thermal Insulation	kg	43.00
Glycol	kg	497.81
Electronics	kg	71.67
Container		
Steel	kg	19279.04
Racks		
Steel	kg	14459.28
Cable		
Copper	kg	153.37
Polyurethane	kg	107.13

Values of this table are collected from GREET [101].

Table A 5. Emission factor database of materials involved in the LCIs of airport hydrogen system components.

Item	CO_2-eq kg/kg	Note	Ref
Acetic acid	0.36		a
Acrylic acid	4.88		a
Active material	19.49	Assume NMC(111)	a
Al Metallization paste	4.44		a
Alkylbenzene sulfonate	3.56	Assume from petroleum	b
Aluminium	5.31	Assume extruded AL from GREET	a
Ammonia	1.96		a
Argon	0.00	Data unavailable	
Au	108.79		a
Back Metallization paste	58.24		a
Brass	3.11		a
Carbon Steel	2.01	Assume Steel	a
Cast Iron	0.39		a
CeO2	17.63	Available on GREET	a
Ceramic	0.82	Assume as Procelain on Greet	a
Chromium steel	10.91	Assume Fe-24% Cr Alloy	a
CO2	1.00		a
Concrete	0.09		a
Copper	2.77		a
Di Water	0.80		c
Dimethyl Carbonate	0.09		a
DGME	4.32	Assume glycol	a
Elastomer	3.23		a
Electricity	0.39		d
Electronics	2.56		a
Ethelene glycol	4.32	Assume glycol	a
Ethylene Carbonate	0.02		a
Fiberglass	1.48		a

Front Metallization paste	72.09		a
Glass	1.42		a
Glycol	4.32		a
Graphite	3.33		a
HDPE	0.94		a
Hexanol	0.53	Assume isopropanol	a
Hydrochloric acid	0.80		a
Hydrogen flouride	1.35		a
Iridium	108.79		a
Isopropanol	0.53		a
Lime	1.14		a
LiPF6	8.13		a
Methanol	0.33		a
Nafion	1.02		a
Natural gas	0.06		c
Nitric acid	0.61		a
Nitrogen	0.14		a
Oil	2.82		a
PET	1.83	Same as Mylar in GREET model	a
Phosphoryl chloride	3.39		c
Plastic	1.88	Assume PVC	a
Polyurethane	2.45		a
PP	1.26		a
Pt	24.17		a
PTFE	6.72		a
Rubber	3.23		a
SGL Carbon	14.40		a
Silane	29.70		a
Silicon	27.50	Assume US solar grade silicon	a
Sodium hydroxide	0.83		a
Stainless Steel	0.68		a
Steel	2.01		a

Sulfuric acid	0.04		a
Thermal Insulation	1.64		a
Titanium	36.95		a
Vulcan XC-72	2.38	Assume Carbon black	c
Water	0.03	Assume tap water	c
Wood	0.00		a
Zeolite	0.00	Data unavailable	
Zinc	2.04		a

a. These data values are adopted from the GREET database [101].
b. The emission factor of Alkylbenzene sulfonate is adopted from [111].
c. These values are presented in [112].
d. The value is collected from [113].

Appendix B. Supplementary Sensitivity Analysis Results

Table B 1. Results of liquefaction unit sizing, LH2 storage capacity and EIS from sensitivity analyses.

Unit cost of GH2 storage ($/kg)	20 (Base)	40	80	160	320	500					
Liquefaction (tpd)	14.19	14.19	14.19	14.19	14.19	14.19					
LH2 Storage (t)	3.42	3.42	3.42	3.42	3.42	3.42					
EIS	0.80	0.70	0.67	0.61	0.60	0.57					
Electrolyzer Efficiency	**50%**	**60%**	**70% (Base)**	**80%**							
Liquefaction (tpd)	14.19	14.19	14.19	14.19							
LH2 Storage (t)	3.42	3.42	3.42	3.42							
EIS	0.81	0.80	0.80	0.79							
Unit cost of electrolyzer ($/kg)	**+50%**	**+40%**	**+30%**	**+20%**	**+10%**	**Base Case**	**-10%**	**-20%**	**-30%**	**-40%**	**-50%**
Liquefaction (tpd)	14.19	14.19	14.19	14.19	14.19	14.19	14.19	14.19	14.19	14.19	14.19
LH2 Storage (t)	3.42	3.42	3.42	3.42	3.42	3.42	3.42	3.42	3.42	3.42	3.42
EIS	0.54	0.54	0.54	0.54	0.61	0.80	0.81	0.83	0.83	0.86	0.98
Unit cost of PV ($/kg)	**+50%**	**+40%**	**+30%**	**+20%**	**+10%**	**Base Case**	**-10%**	**-20%**	**-30%**	**-40%**	**-50%**
Liquefaction (tpd)	14.19	14.19	14.19	14.19	14.19	14.19	14.19	14.19	14.19	14.19	14.19
LH2 Storage (t)	3.42	3.42	3.42	3.42	3.42	3.42	3.42	3.42	3.42	3.42	3.42
EIS	0.47	0.50	0.52	0.53	0.66	0.80	0.81	0.82	0.84	0.85	0.94
Unit cost of WT ($/kg)	**+50%**	**+40%**	**+30%**	**+20%**	**+10%**	**Base Case**	**-10%**	**-20%**	**-30%**	**-40%**	**-50%**
Liquefaction (tpd)	14.19	14.19	14.19	14.19	14.19	14.19	14.19	14.19	14.19	14.19	14.19
LH2 Storage (t)	3.42	3.42	3.42	3.42	3.42	3.42	3.42	3.42	3.42	3.42	3.42
EIS	0.30	0.34	0.44	0.50	0.52	0.80	0.81	0.84	0.88	0.98	0.95